Journal of Cleaner Production 529 (2025) 146801

Contents lists available at ScienceDirect

Journal of Cleaner Production

journal homepage: www.elsevier.com/locate/jclepro

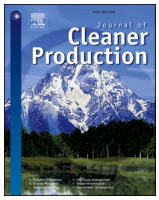

Study on functional group evolution mechanisms and chemical kinetics during gas coal oxygen-free pyrolysis: Insights from high-temperature in-situ FTIR

Guangyu Bai [a,b,c], Haihui Xin [a,b,c,*], Pengcheng Zhang [a,b,c], Chao Luo [a,b,c], Jinliang Li [d], Qiang Zeng [e], Bekir Genc [f], Moshood Onifade [g], Deming Wang [a,b,c]

[a] School of Safety Engineering, China University of Mining and Technology, Xuzhou, 221116, China
[b] Key Laboratory of Gas and Fire Control for Coal Mines, China University of Mining and Technology, Xuzhou, 221116, China
[c] State Key Laboratory of Coal Mine Disaster Prevention and Control, China University of Mining and Technology, Xuzhou, 221116, China
[d] College of Safety Science and Engineering, Anhui University of Science and Technology, Huainan, 232001, China
[e] School of Ecology and Environment, Xinjiang University, Urumqi, 830046, China
[f] School of Mining Engineering, Faculty of Engineering and the Built Environment, University of the Witwatersrand, Johannesburg, 2050, South Africa
[g] Institute of Innovation, Science and Sustainability, Federation University Australia, Ballarat, VIC, 3350, Australia

ARTICLE INFO

Keywords:
Gas coal
In-situ infrared
Correlation
Functional group evolution
Kinetic

ABSTRACT

Gas coal serves as a high-quality raw material for oxygen-free pyrolysis processes in the coal chemical industry, and its pyrolysis has significant implications for alleviating the global energy crisis. However, the complex microscopic chemical reaction mechanisms underlying coal oxygen-free pyrolysis remain poorly understood, representing a critical knowledge gap. In this study, a high-temperature in-situ infrared testing system combined with a two-step dual-band baseline correction method was employed to elucidate the correlation between typical functional groups (11 types) and mass loss conversion rates, investigate the evolution differences of functional groups during oxygen-free pyrolysis of gas coal under the influence of coal rank variations (long-flame coal and lignite) and time-scale effects, and to analyze the kinetic mechanisms of active groups during oxygen-free pyrolysis of gas coal. The results demonstrate that oxygen-containing functional groups act as the triggering mechanism for coal oxygen-free pyrolysis. Aliphatic hydrocarbons exhibit a strong correlations with increased gas coal mass conversion rates, although this relationship gradually transitions to oxygen-containing functional groups in later stages. With decreasing coal rank, the onset temperature of rapid consumption for all functional groups decreased. Time-scale effects predominantly impact the later stages of gas coal oxygen-free pyrolysis, shifting the characteristic transition parameters (e.g., rapid consumption onset, maximum consumption rate temperature) and group conversion rates toward higher temperatures as heating rates increase. The magnitude of the apparent activation energy during oxygen-free pyrolysis primarily depends on the difficulty of the initial bond cleavage and the efficiency of subsequent chain reactions. The high activation energy of benzene rings (269.6 kJ/mol) reflects the formation of semi-coke and coal char structural frameworks, adhering to a first-order reaction mechanism. The elevated activation energy of C-O-C consumption stages (338.6 kJ/mol) incorporates synergistic contributions from chemical bond cleavage and diffusion resistance. Aliphatic hydrocarbons follow a random nucleation and nuclei growth mechanism, while other functional groups are governed by diffusion models. These findings enrich the understanding of coal oxygen-free pyrolysis mechanisms, provide critical insights for coal chemical engineers, and provide theoretical insights into the advancement of clean and efficient technologies for the utilization of low-rank coal.

* Corresponding author. School of Safety Engineering, China University of Mining &Technology, China.
E-mail address: xinxhh@cumt.edu.cn (H. Xin).

https://doi.org/10.1016/j.jclepro.2025.146801
Received 1 July 2025; Received in revised form 28 August 2025; Accepted 5 October 2025

1. Introduction

Currently, coal accounts for 37 % of global electricity generation (Pope et al., 2024). Gas coal, a low-rank bituminous coal characterized by a high volatile content (>37 %) and strong caking properties, serves as both a crucial component in coking blends and an ideal feedstock for coal pyrolysis processes in chemical industries (Huang et al., 2025; Umar et al., 2024; Xu et al., 2024). However, extensive exploitation and utilization of coal resources have resulted in significant environmental challenges (Gopinathan et al., 2023; Lak et al., 2024). In China, particulate matter and greenhouse gas emissions from coal combustion have become the primary drivers of regional air quality deterioration and climate change (Deng et al., 2023; Li et al., 2024). This has driven substantial interest in efficient clean coal conversion technologies, particularly pyrolysis, as a potential solution for sustainable energy development.

Oxygen-free pyrolysis, as a critical step in the thermal conversion of low-rank coal (Li, S. et al., 2025a,b; Ma et al., 2023). It acts not only as a precursor process for combustion and gasification, but also directly governs tar yield and pollutant formation pathways through complex functional group evolution (e.g., aliphatic chain cleavage and oxygen-containing group decomposition) (Keboletse et al., 2021; Shi et al., 2024; Zhang et al., 2025). Consequently, in-depth investigation of microstructural changes during coal oxygen-free pyrolysis and revealing the mechanisms of functional group evolution during this process can not only provide theoretical support for optimizing pyrolysis processes and improving coal conversion efficiency, but also pave the way for fundamental research on coalification processes.

Current analytical techniques for characterizing functional group distributions in coal primarily include Fourier Transform Infrared Spectroscopy (FTIR) and $^{1}H/^{13}C$ Nuclear Magnetic Resonance (NMR) (Cai et al., 2023; Li et al., 2023). Among these, FTIR has become the predominant method for coal structural analysis because of its operational simplicity and cost-effectiveness, with extensive applications in determining the functional group composition, degree of coalification, and genetic classification (Wu et al., 2023). FTIR spectroscopy is particularly effective in determining the carbon-hydrogen ratios and heteroatomic functional group distributions (Mishra et al., 2023). Pan et al. (2020) investigated the evolution of functional groups in coal under oxygen-free and aerobic environments using FTIR, revealing that hydroxyl (-OH) groups exhibit significantly greater peak heights and areas under oxygen-free conditions, indicating the critical role of -OH in coal oxidation processes. Lin et al. (2014) analyzed functional group transformations during lignite pyrolysis in oxygen-free pyrolysis using FTIR, demonstrating progressive decomposition of aliphatic groups with increasing temperature, while aromatic bonds maintained higher stability below 700 °C. However, the functional group evolution data reported in these studies predominantly rely on non-in-situ samples, which cannot directly reflect the real-time structural changes in coal during heating. In contrast, in situ FTIR technology enables the real-time monitoring of functional group dynamics while eliminating secondary interference from cooling procedures or sample preparation (Xiong et al., 2015). Qi et al. (2014) conducted a comparative analysis of in-situ and non-in-situ FTIR techniques to investigate the chemical changes in surface functional groups during the low-temperature oxidation of coal. Their findings conclusively demonstrated that that in-situ FTIR data can more accurately reflect changes in functional groups. Zhang et al. (Zhang, Q.L. et al., 2024a,b) utilized in situ FTIR to analyze the characteristics and quantitative changes in functional groups during coal oxygen-free pyrolysis, revealing the following order of mass fractions: aliphatic > •OH > aromatic C–H > C–O > C=C > C=O. Niu et al. (2016) utilized in-situ FTIR to investigate the changes in major functional groups during the pyrolysis of perhydrous bituminous coal and found that the decomposition of aliphatic groups dominated the primary pyrolysis of perhydrous coal.

Despite this, in situ FTIR still faces significant challenges: (1) The spectra obtained from in situ FTIR exhibit baseline drift with temperature and wavenumber variations, making it difficult to effectively analyze changes in specific functional groups; (2) Most existing studies are limited to temperatures below 500 °C (Jia et al., 2025; Li, Y. et al., 2025a,b; Zhang, X. et al., 2024a,b; Zhao et al., 2023), while their analyses of functional group evolution at low temperatures remain simplistic, neglecting correlations with coal pyrolysis mass loss. Xu et al. (2016) extended the testing temperature to 1000 °C using the Infrared Microscopy beamline facility at Australian Synchrotron, but its high equipment cost hinders industrial applications; (3) The influence of heating rates and coal rank on the dynamic evolution of functional groups has not been systematically resolved. Additionally, kinetics are intrinsically linked to the reaction mechanisms underlying thermal conversion processes, with kinetic data serving as fundamental theoretical support for the design of thermal conversion reactors. Traditionally, kinetic parameters have been predominantly obtained by calculating the conversion rates from the mass loss percentages derived from thermogravimetric data. However, with the exception of the studies by Niu (Niu et al., 2016), Zhao (Zhao et al., 2023) and Li (Wen et al., 2011), there remains a notable scarcity of research employing quantitative functional group analysis to evaluate kinetic characteristics.

This study focuses on gas coal from the Donglutian Mine in Shanxi, China. By employing a novel high-temperature in situ infrared testing method, the baseline drift in infrared spectra is effectively resolved, enabling systematic exploration of the following scientific issues: (1) The microscopic mechanisms of functional group evolution during oxygen-free pyrolysis of gas coal under the influence of temperature (30–630 °C), coal rank variations (long-flame coal, lignite), and time-scale effects (heating rates: 2, 5, 10 °C/min); (2) Elucidation of the correlation between functional group evolution and stage development during oxygen-free pyrolysis of gas coal; (3) Revelation of the kinetic characteristics of active groups in gas coal during oxygen-free pyrolysis. The innovation of this study lies in integrating stage development correlations, coal rank differences, time-scale effects, and kinetic parameters into a unified analytical framework for the first time. This provides novel theoretical tools for optimizing coal pyrolysis processes and controlling pollutants at the source, thereby advancing the development of clean and efficient coal utilization technologies.

2. Experiments and methods

2.1. Coal sample

The gas coal samples investigated in this study were collected from the Pingshuo Coal Mine in Shanxi, China. In accordance with Chinese National Standard GB474-2008 (Method for preparation of coal samples), the crushed coal samples were sieved through 200–300 mesh (0.050–0.075 mm), followed by drying at 40 °C and subsequent hermetic storage. Proximate analysis was conducted using an SDTGA5000 analyzer, and ultimate analysis was performed using a Vario MICRO elemental analyzer. The test results are listed in Table 1.

2.2. Stage division methods

To investigate the real-time evolution laws of the functional groups during the oxygen-free pyrolysis of coal, mass loss data were acquired using an SDT-Q600 thermogravimetric analyzer. Coal samples weighing approximately 5 mg were heated from 30 °C to 800 °C at a rate of 2 °C/min under a constant nitrogen flow of 100 mL/min. The progression of coal oxygen-free pyrolysis was quantified using the mass loss conversion rate ϑ (Aprianti et al., 2023), defined as $\vartheta = (m_0 - m_t)/(m_0 - m_{end})$, where m_0, m_t, and m_{end} represent the initial mass, instantaneous mass at time t, and final mass at the terminal temperature, respectively. The relationship between the temperature (x-axis) and mass loss conversion rate (y-axis) is plotted in Fig. 1. The oxygen-free pyrolysis process of gas

Table 1
Proximate and ultimate analyses of gas coal.

Proximate Analysis (wt.%)				Ultimate Analysis (wt.%)				
M_{ad}	A_d	V_d	FC_d	C	H	O	N	S
2.23	17.93	37.19	42.65	62.10	4.878	32.02	0.231	0.812

Note: M_{ad}-Moisture, A_d-Ash, V_d-Volatile, FC_d-Fixed carbon.

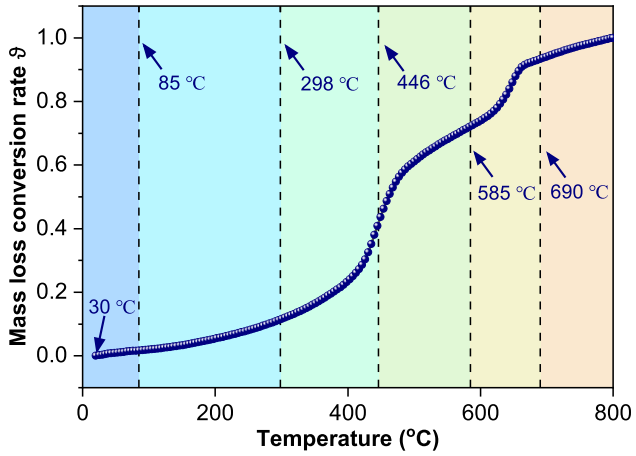

Fig. 1. Stage division under the influence of conversion rate.

coal exhibits five distinct stages: rapid drying and degassing (30–85 °C, Stage I), sustained slow degassing (85–298 °C, Stage II), colloid formation (298–446 °C, Stage III), semi-coke formation (446–585 °C, Stage IV), and char formation (585–690 °C, Stage V), with Stages III and IV representing the thermal decomposition phase (Bai et al., 2025).

2.3. Infrared spectroscopy testing

In this study, functional group analysis was conducted using a Nicolet 6700 Fourier transform infrared spectrometer (Thermo Fisher Scientific Inc., USA) equipped with an in-situ reaction cell and water cooling system. Prior to testing, the instrument was preheated and the detector was cooled with liquid nitrogen. The infrared spectral intensity was calibrated, and KBr powder was prepared for the KBr background reference collection. To ensure uniform heating of the coal sample during high-temperature pyrolysis, three layers of high-temperature-resistant thermally conductive metal spacers were installed in the diffuse reflectance cell, with a thin layer of coal sample evenly spread on the top, as illustrated in Fig. 2. To fully span the pyrolysis decomposition stage under oxygen-free pyrolysis conditions, samples were heated from 30 to 630 °C at heating rates of 2, 5, and 10 °C/min (total acquisition time: 60 min). The heating rate of 2 °C/min allowed for more thorough oxygen-free pyrolysis of the coal and was used as the benchmark for studying time-scale effects. A nitrogen flow rate of 30 mL/min was maintained throughout the experiments. Measurements were performed in the diffuse reflectance mode with the following parameters: 64 scans per sample, 4 cm^{-1} resolution, wavenumber range of 650–4000 cm^{-1}, and y-axis data expressed in Kubelka-Munk (KM) units. Three replicate tests were conducted at each heating rate to ensure reliability.

2.4. Two-step dual-band baseline correction method

The baseline of the in situ three-dimensional infrared spectra was affected by prolonged testing and experimental heating, leading to baseline drift across different wavenumbers and temperatures. To accurately analyze the evolution of functional groups in coal during oxygen-free pyrolysis, this study employed the OMNIC software. First, based on the analysis of the correction fitting orders of 1, 2, 3, 4, 5, and 6 in the coal quantitative analysis, it was found that the baseline correction for the overall coal structure across the wavenumber range of 400–4000 cm^{-1} did not yield satisfactory results. Thus, the infrared spectrum of coal is divided into two bands at 2050 cm^{-1}: 2050–4000 cm^{-1} and 400–2050 cm^{-1}. Baseline drift characteristics were determined by analyzing spectral shifts in the non-characteristic peak regions (3900–4000 cm^{-1} and 1950–2050 cm^{-1}). Subsequently, corrections were applied separately to the wavenumber- and temperature-dependent drifts. A two-step baseline correction process ultimately yielded the optimized spectra. The detailed methodology aligns with a previous study by the same authors (Bai et al., 2024).

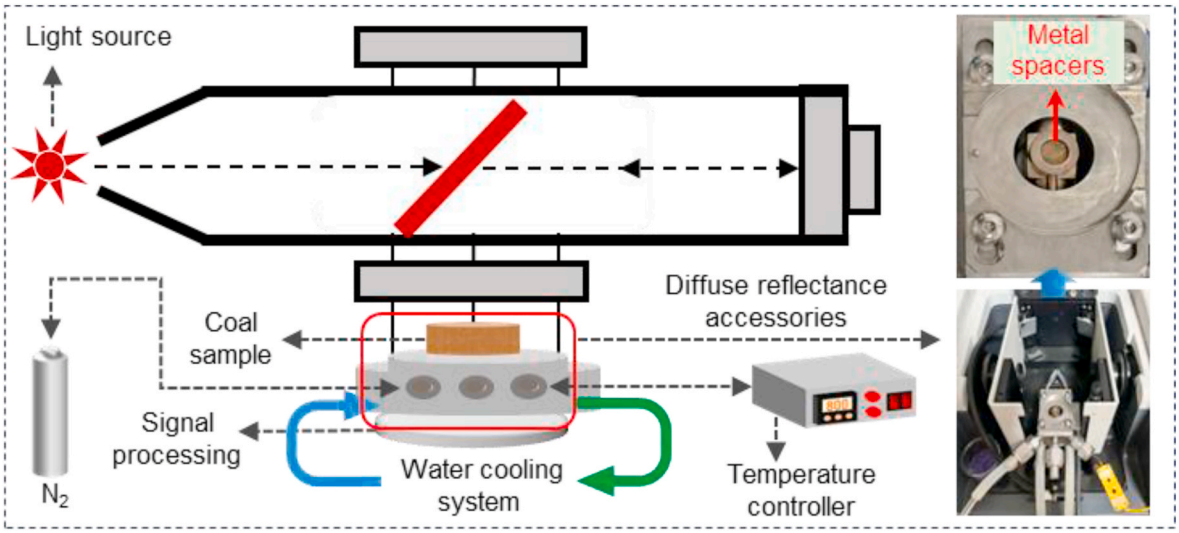

Fig. 2. Schematic diagram of high-temperature in situ diffuse reflectance infrared spectroscopy.

2.5. Kinetic methods

The Coats-Redfern method, first proposed in 1964, is one of the most versatile model fitting approaches (Çepelioğullar et al., 2016). As an integral method, it enables the determination of the activation energy and reaction mechanisms without prior knowledge of reaction kinetics. It offers a simple and model-independent approach, making it particularly advantageous for handling complex reactions or situations in which the reaction mechanism is not well understood (Hameed et al., 2024). Although it has traditionally been used to extract kinetic parameters from thermogravimetric data (Isah et al., 2025), this study attempted to utilize KM values to calculate the kinetic parameters of the samples, thereby exploring the reaction mechanisms of the active functional groups at different temperatures.

The conversion rate, α, which represents the extent of the reaction for the consumption or generation of different functional groups at a certain moment, is expressed by Equation (1):

$$\alpha = \frac{KM_0 - KM_t}{KM_0 - KM_\infty} \tag{1}$$

where KM_0, KM_t and KM_∞ are the KM values at the initial time, time t, and end of the experiment, respectively.

The rate equation for the solid thermal decomposition can be expressed as Equation (2) (Rego et al., 2020):

$$\frac{d\alpha}{dT} = \frac{A}{\beta} exp\left(\frac{-E_a}{RT}\right) f(\alpha) \tag{2}$$

where T is the thermodynamic temperature, in K, A is the pre-exponential factor, in min^{-1}, β is the heating rate, in K/min, E_a is the activation energy, in kJ/mol, and R is the universal gas constant (8.314 J/(mol·K)).

By transforming Equation (2), multiplying both sides by $\frac{1}{T^2}$, and integrating, Equation (3) is obtained:

$$\int_0^\alpha \frac{d\alpha}{f(\alpha)T^2} = \int_{T_0}^{T} \frac{A}{\beta} exp\left(\frac{-E_a}{RT}\right) \frac{1}{T^2} dT = \frac{AR}{\beta E_a}\left[exp\left(\frac{-E_a}{RT}\right)\right] - exp\left(-\frac{E_a}{RT_0}\right) \tag{3}$$

Taking the logarithm of both sides of Equation (3), where $exp\left(-\frac{E_a}{RT_0}\right) \approx 0$, i.e., the Coats-Redfern method equation is formula (4) (Coats and Redfern, 1964):

$$ln\frac{g(\alpha)}{T^2} = ln\left(\frac{AR}{\beta E_a}\right) - \frac{E_a}{RT} \tag{4}$$

When studying the kinetic characteristics of coal oxygen-free pyrolysis reactions using non-isothermal methods, different reaction mechanism functions have different forms. Table 2 summarizes the 21 commonly used reaction mechanism functions.

For different reaction mechanism functions, by defining $y = ln\frac{g(\alpha)}{T^2}$ and $x = \frac{1}{RT}$, the relationship between y and x can be plotted using Equation (4). Linear regression fitting yields a straight line with a slope of $-E_a$, from which the activation energy E_a of the functional group reaction can be calculated. The correlation coefficient (R^2) was used to evaluate the linear fit of the model, facilitating the selection of the best-fitting model as the optimal reaction mechanism.

3. Results and discussion

3.1. Functional groups in raw coal samples

The 3D infrared spectra obtained during the oxygen-free pyrolysis process of gas coal were corrected for the baseline drift at different wavenumbers. The corrected results are shown in Fig. 3.

Table 2
Common reaction mechanism functions (Hu and Shi, 2008; Hu et al., 2005; Vlaev et al., 2003).

$g(\alpha)$	Reaction type	Reaction mechanism	Function
$g(\alpha)$ 1	Chemical reaction	First-order reaction	$-ln(1-\alpha)$
$g(\alpha)$ 2		Second-order reaction	$(1-\alpha)^{-1} - 1$
$g(\alpha)$ 3		Third-order reaction	$\left[(1-\alpha)^{-2} - 1\right]/2$
$g(\alpha)$ 4	Exponential nucleation	Power law, n = 1/2	$\alpha^{1/2}$
$g(\alpha)$ 5		Power law, n = 1/3	$\alpha^{1/3}$
$g(\alpha)$ 6		Power law, n = 1/4	$\alpha^{1/4}$
$g(\alpha)$ 7	Diffusion model	One-dimensional diffusion (Parabolic law)	α^2
$g(\alpha)$ 8		Two-dimensional diffusion (Valensi equation)	$\alpha + (1-\alpha)ln(1-\alpha)$
$g(\alpha)$ 9		Three-dimensional diffusion (Jander equation), n = 2	$\left[1-(1-\alpha)^{1/3}\right]^2$
$g(\alpha)$ 10		Three-dimensional diffusion (Ginstling-Brounshtein equation)	$1 - 2\alpha/3 - (1-\alpha)^{2/3}$
$g(\alpha)$ 11	Shrinking core model	Contraction	$(1-\alpha)^{-1/2}$
$g(\alpha)$ 12		Phase boundary reaction, n = 1/2	$1-(1-\alpha)^{1/2}$
$g(\alpha)$ 13		Phase boundary reaction, n = 1/3	$1-(1-\alpha)^{1/3}$
$g(\alpha)$ 14		Phase boundary reaction, n = 2	$1-(1-\alpha)^{2}$
$g(\alpha)$ 15		Phase boundary reaction, n = 3	$1-(1-\alpha)^{3}$
$g(\alpha)$ 16		Phase boundary reaction, n = 4	$1-(1-\alpha)^{4}$
$g(\alpha)$ 17	Random nucleation and growth	Avrami-Erofeev model, n = 1/2	$[-ln(1-\alpha)]^{1/2}$
$g(\alpha)$ 18		Avrami-Erofeev model, n = 1/3	$[-ln(1-\alpha)]^{1/3}$
$g(\alpha)$ 19		Avrami-Erofeev model, n = 2	$[-ln(1-\alpha)]^{2}$
$g(\alpha)$ 20		Avrami-Erofeev model, n = 3	$[-ln(1-\alpha)]^{3}$
$g(\alpha)$ 21		Avrami-Erofeev model, n = 4	$[-ln(1-\alpha)]^{4}$

As shown in Fig. 3, after baseline drift correction at different wavenumbers, the baselines of the infrared spectra remained horizontal within identical wavenumber ranges. However, baseline drift still occurred in the peak intensities or areas of the functional groups in the 3D infrared spectra as the temperature changed, manifesting as an overall spectral shift toward higher or lower intensities. Fig. 4 shows the 3D real-time infrared spectral projection of gas coal during oxygen-free pyrolysis. Fig. 5 presents the drift curve at the baseline point (3980 cm^{-1}) with increasing temperature, along with the original and baseline-corrected curves of the -CH_3 group. It is evident that the original curve of the -CH_3 group in gas coal initially exhibits a continuous decline, followed by a rapid increase in the later stages. However, the actual intensity of the -CH_3 group continued to decrease. This discrepancy arises mainly from the thermal baseline drift, which obscures true spectral signals. Therefore, rigorous baseline correction is essential to uncover authentic chemical behavior.

The content of different functional groups in the coal molecular structure varies, which is reflected in the infrared spectra as differences in vibrational intensities. According to Fig. 3, during the heating process, spectral changes mainly occurred in the 3700–2800 cm^{-1} and 1800–1200 cm^{-1} bands, where all four major categories of functional groups present in the coal structure were involved. Owing to the

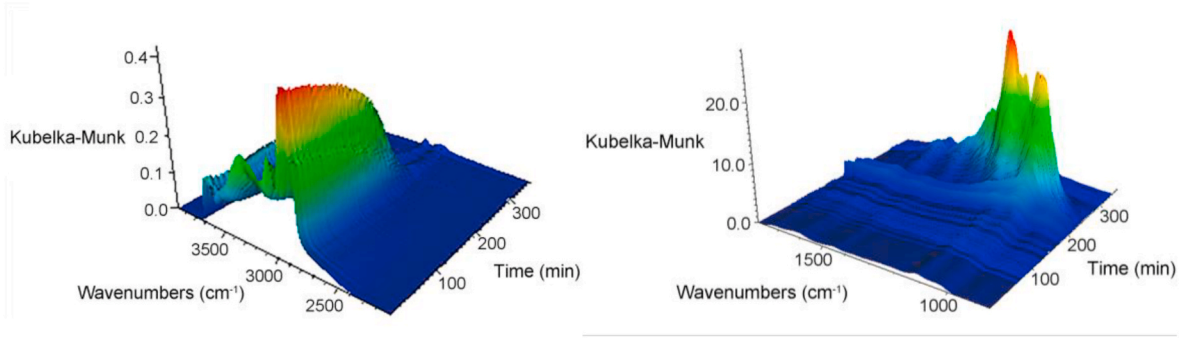

Fig. 3. 3D real-time infrared spectra of gas coal during oxygen-free pyrolysis at a heating rate of 2 °C/min.

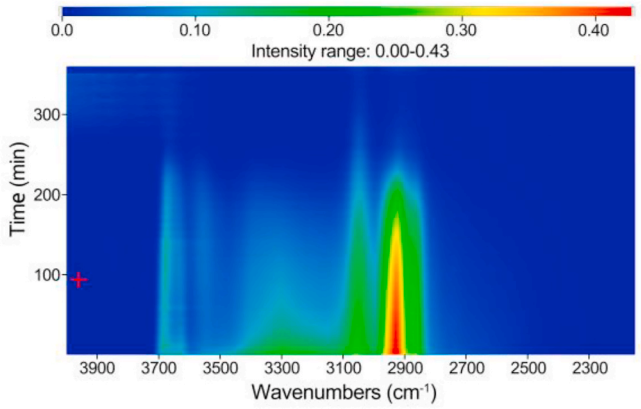

Fig. 4. Projection of infrared 3D spectra with the range of 4000-2000 cm^{-1}.

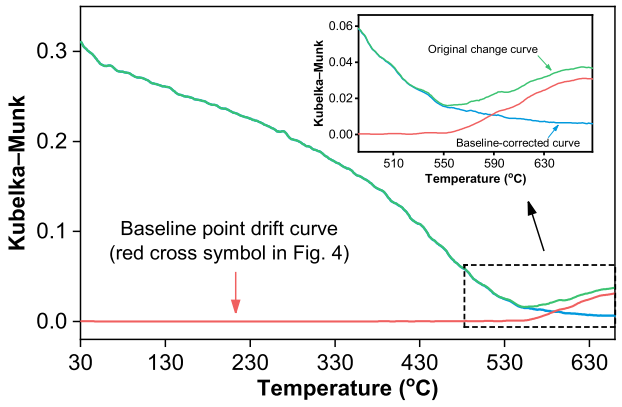

Fig. 5. Baseline drift and correction of methyl asymmetric stretching vibration.

complex nature of coal as a mixture, the absorption peaks tend to overlap. Therefore, the characteristic absorption peaks of the four types of functional groups were deconvoluted using the OMNIC software, and the results are shown in Fig. 6. The assignments of the active functional groups in coal are summarized in Table 3 (Dai et al., 2023; Wang, 2012; Zheng et al., 2020). Based on the calculation of the peak areas, the relative abundance of functional groups in the coal sample was determined to be oxygen-containing functional groups (39.66 %) > aromatic hydrocarbons (34.68 %) > aliphatic hydrocarbons (17.79 %) > hydroxyl groups (7.87 %), with benzene rings accounting for 27.22 % and C–O–C groups at 22.54 %. The high content of oxygen-containing functional groups and aromatic hydrocarbons in gas coal contributes to its high volatile matter content and strong thermoplasticity during pyrolysis, making it an ideal feedstock for coking and coal-to-chemical processes.

3.2. Correlation characteristics of stage-wise functional group evolution during oxygen-free pyrolysis of gas coal

3.2.1. Stage evolution laws of functional groups

Through baseline drift correction, this study acquired real-time infrared spectral evolution curves of distinct functional groups during oxygen-free pyrolysis of gas coal at a heating rate of 2 °C/min, the corresponding results shown in Fig. 7(a) and (b).

From Fig. 7(a), it is evident that the reduction in aliphatic hydrocarbons and Ar-CH groups is most pronounced, with nearly all functional groups, except Ar-CH, being entirely depleted by the end of oxygen-free pyrolysis. Fig. 7(b) reveals an increase in the aromatic C=C stretching vibrations (benzene rings) during the later stages of oxygen-free pyrolysis. This is attributed to the formation of aromatic rings through dehydrogenation and rearrangement of chain-like hydrocarbon structures, as well as the condensation of existing aromatic compounds, as illustrated in reactions (Model 1) and (Model 2), leading to the formation of denser polycyclic aromatic hydrocarbons (PAHs). The increase in C-O-C is even more pronounced, which is believed to be mainly influenced by mineral phase transitions during the oxygen-free pyrolysis of coal. In addition, a substantial amount of C-O-C was generated during the process itself, as the phenolic hydroxyl groups (Ar-OH) underwent dehydration and condensation at high temperatures to form aryl ethers (Ar-O-Ar), as shown in reaction (Model 3). It is also possible that the chain-like ether structures were converted into more stable oxygen-containing aromatic heterocycles, such as dibenzofuran, through structural rearrangement, as shown in reaction (Model 4), leading to a simultaneous increase in both C-O-C and aromatic structures, thereby intensifying infrared absorption.

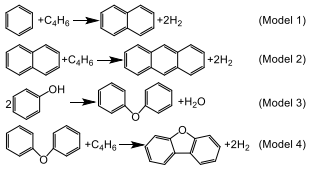

To further quantify the detailed evolutionary laws of the functional groups during oxygen-free pyrolysis, the infrared intensity changes within specific temperature intervals were calculated using Equation (5), and the results are summarized in Table 4.

$$L_i = \left(\frac{KM_S}{KM_0} - \frac{KM_F}{KM_0}\right) \times 100\% \ (i = 1, 2, \cdots, m) \quad (5)$$

Where L_i represents the percentage change in the infrared intensity for the i-th temperature interval, $KM_0$is the initial infrared intensity value, KM_S and KM_F denote the infrared intensity values at the beginning and end of the i-th temperature interval, respectively. A positive L_i value indicates a decrease in the infrared intensity, whereas a negative L_i value indicates an increase.

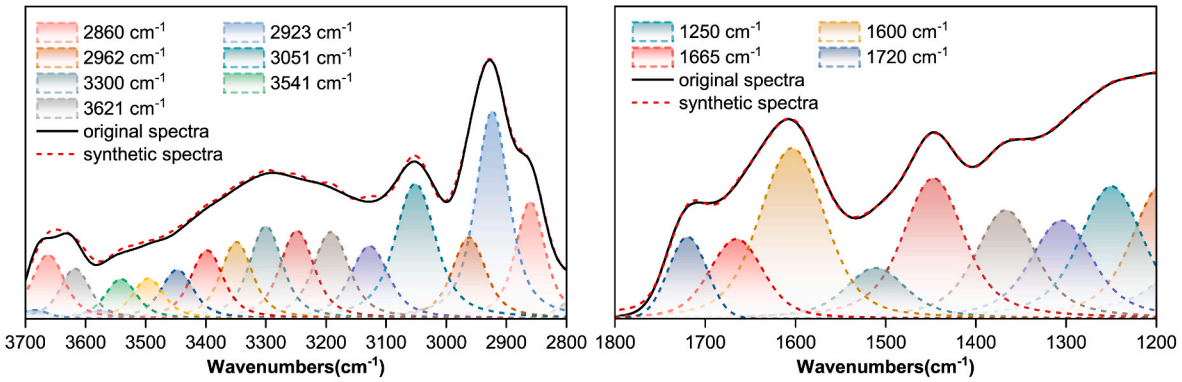

Fig. 6. Peak fitting curves of the coal sample in different spectral bands.

Table 3
Infrared absorption peak assignment of main functional groups in coal.

No.	Peak Position (cm^{-1})	Functional Group	Group Type
1	1250	C-O-C	Phenoxy deformation
2	1600	C=C	Aromatic C=C stretching vibration
3	1665	C=O	Carbonyl stretching vibration
4	1720	-COOH	Carboxyl stretching vibration
5	2860	$-CH_2-$	Methylene symmetric stretching vibration
6	2923	$-CH_2-$	Methylene asymmetric stretching vibration
7	2962	$-CH_3$	Methyl asymmetric stretching vibration
8	3051	Ar-CH	Aromatic CH stretching vibration
9	3300	-OH	Water associated hydroxyl
10	3541		Phenolic alcohol associated hydroxyl
11	3621		Free hydroxyl

(1)During the rapid drying and degassing stage (temperature <85 °C), the primary changes in gas coal involve a reduction in the quantity of associated hydroxyl groups due to dehydration, alongside a significant decrease in the spectral intensity of free hydroxyl groups. The spectral intensities of aliphatic hydrocarbons and Ar–CH groups also gradually diminished with increasing temperature during oxygen-free pyrolysis. Notably, the Ar–CH group serves as an indicator of aromatic ring stability; the weaker vibrational intensity of Ar–CH correlates with a higher aromatic stability and lower reactivity with oxygen. The spectral intensities of the benzene rings in the aromatic hydrocarbons remained largely unchanged, indicating that the aromatic skeleton of the coal remained intact. Among the oxygen-containing functional groups, the spectral intensity of the C=O groups showed a slight decrease, while -COOH exhibited a minor increasing trend, although both remained relatively stable overall. The spectral intensities of the C-O-C groups remained constant.

(2) During the sustained slow degassing stage (85 °C < temperature <298 °C), moisture drying in gas coal under oxygen-free pyrolysis was nearly complete, but water associated hydroxyl groups continued to decrease. The phenolic alcohol associated hydroxyl and free hydroxyl groups remained largely stable. The infrared intensity of aliphatic hydrocarbons continues to decline. The trends for aromatic hydrocarbons and C-O-C resemble those observed during the rapid drying stage. C=O showed a slight increase, likely due to the conversion of aliphatic hydrocarbons, while -COOH decreased marginally. Overall, oxygen-containing functional groups exhibited slow changes during this stage, attributed to the predominant removal of native gases from the coal matrix and residual moisture, resulting in minimal impact on the absorbance of the coal structural groups. It is noteworthy that this stage persisted until the release of volatile components began.

(3) During the colloid formation stage (298 °C < temperature <446 °C), the oxygen-free pyrolysis process of gas coal enters the initial stage of thermal decomposition, with the process being dominated by colloid formation. Key characteristics include the fracture of weak bonds, with broken fragments forming liquid tar that is retained within the coal structure. The infrared intensity of

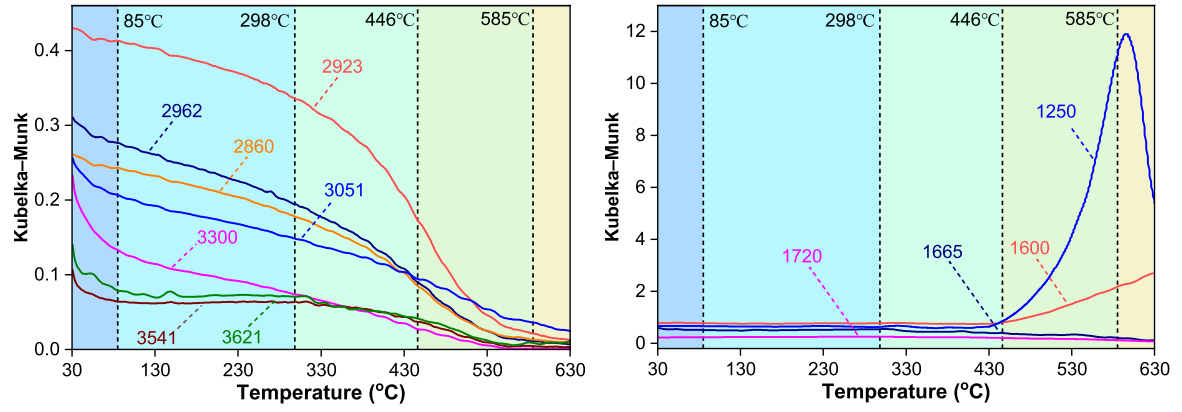

Fig. 7. Real-time evolution curves of different functional groups with increasing temperature.

Table 4
Stage evolution laws of functional groups during oxygen-free pyrolysis of gas coal.

Functional group	Stage I	Stage II	Stage III	Stage IV	Stage V
	30–85 °C	85–298 °C	298–446 °C	446–585 °C	585–690 °C
	Evolution laws				
Methyl asymmetric stretching vibration	Continuous decrease by 97.7 %: 30–390 °C: Slow reduction (54.4 %); 390–560 °C: Rapid reduction (41.0 %); 560–630 °C: Slow reduction (2.3 %).				
Methylene asymmetric stretching vibration	Continuous decrease by 97.1 %: 30–380 °C: Slow reduction (36.2 %); 380–550 °C: Rapid reduction (56.5 %); 550–630 °C: Slow reduction (4.4 %).				
Methylene symmetric stretching vibration	Continuous decrease by 96.5 %: 30–385 °C: Slow reduction (47.8 %); 385–554 °C: Rapid reduction (45.6 %); 554–630 °C: Slow reduction (3.1 %).				
Water associated hydroxyl	Complete depletion (100 %): 30–85 °C: Rapid reduction (42.9 %); 85–551 °C: Slow reduction (57.1 %); 567–630 °C: Stable (depleted).				
Phenolic alcohol associated hydroxyl	Continuous decrease by 96.1 %: 30–97 °C: Rapid reduction (40.3 %); 97–316 °C: Stable; 316–556 °C: Rapid reduction (55.8 %); 556–630 °C: Stable.				
Free hydroxyl	Continuous decrease by 97.6 %: 30–124 °C: Rapid reduction (83.4 %); 124–310 °C: Stable; 310–563 °C: Slow reduction (15.2 %); 563–630 °C: Increase (1 %).				
Ar-CH	Continuous decrease by 90.6 %: 30–78 °C: Rapid reduction (18.6 %); 78–430 °C: Slow reduction (40.9 %); 430–558 °C: Rapid reduction (24.6 %); 558–630 °C: Slow reduction (6.5 %).				
Benzene rings	Continuous increase by 242.3 %: 30–430 °C: Stable; 430–630 °C: Rapid increase (242.3 %).				
C=O	Overall decrease by 76.5 %: 30–124 °C: Slow reduction (6.9 %); 124–274 °C: Slow increase (7.3 %); 274–530 °C: Slow reduction (41.5 %); 530–630 °C: Rapid reduction (35.4 %).				
-COOH	Overall decrease by 68.4 %: 30–278 °C: Slow increase (15.6 %); 278–406 °C: Slow reduction (13.4 %); 406–630 °C: Rapid reduction (70.6 %).				
C-O-C	Overall increase of 688.3 %. 30–432 °C: Stable; 432–596 °C: Rapid increase (1660.4 %); 596–630 °C: Rapid decrease (972.1 %).				

aliphatic hydrocarbons transitions to decreased rapidly, whereas aromatic hydrocarbons exhibited trends similar to those observed in the sustained slow degassing stage. The C=O and -COOH groups in the oxygen-containing functional groups showed gradual reductions. Owing to coalification effects, C–O–C groups, which are prone to bond cleavage, begin to form slowly in the later part of this stage. Phenolic alcohol associated hydroxyl and free hydroxyl groups begin to decrease rapidly beyond the 314 °C threshold, which can be considered as the beginning of the breakage of weaker chemical bonds in the coal, leading to the rapid formation of colloids and rapid degassing by thermal decomposition. At the same time, the water associated hydroxyl groups continued to decrease linearly.

(4) During the semi-coke formation stage (446 °C < temperature <585 °C), the oxygen-free pyrolysis of gas coal enters the later phase of thermal decomposition, dominated by rapid thermal decomposition and condensation of colloidal bodies to form semi-coke. The infrared intensity of aliphatic hydrocarbons decreased sharply, primarily because of the extensive fracture of aliphatic side chains during the oxygen-free pyrolysis of coal, generating tar, alkanes, olefins, alkynes, and other gaseous products. Significant decomposition of the C=O and -COOH groups occurs, with their infrared intensities declining rapidly as they gradually form carbon oxides and other gases. Near 446 °C, the Ar–CH group undergoes rapid reduction, while the infrared intensity of benzene rings shifts to a rapidly increase, influenced by thermal effects and the inherent ash structure of coal. Simultaneously, the aromatic skeleton underwent polycondensation reactions, promoting the conversion of monocyclic and bicyclic aromatic hydrocarbons into tricyclic and higher PAHs. Additionally, the infrared intensity of the C-O-C group begins to increase rapidly, indicating that C-O-C, which is easy to break, begins to form rapidly at this stage and is completed in subsequent stages. During this stage, the associated hydroxyl groups decreased rapidly and were nearly completely eliminated. Notably, phenolic alcohol associated hydroxyl hydrogen bonds undergo complete elimination at 556 °C, attributed to the pyrolysis of phenolic hydroxyl groups in coal at high temperatures, which generates phenolic organic compounds. As the temperature further increased, the process transitioned into a sssemi-coke production state.

(5) When the temperature reached 585 °C, the oxygen-free pyrolysis of gas coal primarily entered semi-coke condensation forming coal char stage (Stage V), the infrared intensity of C-O-C groups transitioned to rapid reduction. At 630 °C, the endpoint of in situ infrared testing. Post-630 °C condensation primarily drives changes in residual aromatic hydrocarbons, which accords with the characteristics of the group change caused by the poly-condensation dehydrogenation gas.

In summary, the oxygen-free pyrolysis of coal is highly complex and involves diverse transformations and reactions of different functional groups. During the rapid drying and degassing stage, changes primarily affect the associated hydroxyl groups, which determine the generation of water vapor from coal. The products released during the sustained slow degassing stage were inferred to be mainly water vapor and ammonia. In the more complex thermal decomposition stage, the bridge bonds, aliphatic side chains, and oxygen-containing groups undergo thermal cracking. The early phase of thermal decomposition (298–446 °C) involves the breakdown of readily decomposable oxygen-containing functional groups and bridge bonds, leading to the formation of coal colloids and generation of tar and gases. During this process, the tar is predominantly composed of phenolic organic compounds (oxygen-containing organics), followed by naphthalenic organics (aliphatic hydrocarbons) (Xin et al., 2024b). Small-molecule gases mainly include H_2, CO, CO_2, CH_4, C_2H_2, C_2H_4, and C_2H_6. In the later phase of thermal decomposition (446–585 °C), direct cleavage of aliphatic chains and oxygen-containing groups in the coal colloid structure occurs, along with condensation and solidification between free radicals, the liquid phase, and solid-phase molecular structures during the curing of the coal colloid until semi-coke is formed. Throughout this stage, large quantities of small-molecule gases and tar were generated, and the molecular weight of the phenolic compounds in the tar also increased. Hence, the composition of tar serves as a potential indicator of the coal pyrolysis state. However, the aromatic structure content continues to increase during this process; therefore, the direct generation of CH_4 and C_2H_2 from aromatic structures is minimal, and the formation of CH_4 is mainly determined by the cleavage of methyl groups and hydrogen atoms from the aliphatic side chains. Concurrently with the chemical changes in the coal's inherent structure, further decomposition, dehydrogenation, and condensation reactions occur, involving free radicals from the volatile products of thermal decomposition. At higher temperatures, the

polycondensation of aromatic hydrocarbon structures in semi-coke produces H_2, and the structural ordering of the aromatic entities increases.

3.2.2. Correlation between functional groups and stage conversion rate

The stage development during the oxygen-free pyrolysis of gas coal has a significant impact on the changes in the microscopic groups. Microscopic groups determine the essence of coal reactions, and the mass loss conversion rate determines the extent of the stage development of the oxygen-free pyrolysis of coal. Consequently, an intrinsic interplay exists between the mass loss conversion rate and microscopic functional groups. To investigate the relationship between the microstructure of gas coal and its conversion rate during oxygen-free pyrolysis, the Pearson correlation coefficient method was employed to identify the functional groups that most significantly influenced mass conversion. The Pearson correlation coefficient, defined as the ratio of the covariance to the product of the standard deviations of the two variables X and Y, ranges between −1 and 1. This calculation is given in Equation (6)

$$r = \frac{n\sum X_i Y_i - (\sum X_i)(\sum Y_i)}{\sqrt{[n\sum X_i^2 - (\sum X_i^2)]\,[n\sum Y_i^2 - (\sum Y_i^2)]}} \tag{6}$$

where n is the sample size, and X and Y are the observed values of the two variables. A value closer to 1 indicates a stronger positive correlation between the conversion rate and a specific functional group, whereas a value closer to −1 signifies a stronger negative correlation. The results are shown in Fig. 8.

As shown in Fig. 8, during the full-stage analysis, the correlation coefficients exceeded ±0.8. However, the influence of different functional groups on the oxygen-free pyrolysis of coal varied significantly across different stages. In stage I, the three functional groups with the greatest correlation were methyl asymmetric stretching vibration, Ar-CH, and water associated hydroxyl; in stage II, the three functional groups with the greatest correlation were mainly aliphatic hydrocarbons; in stage III, the three functional groups with the greatest correlation were mainly methylene asymmetric stretching vibration, methylene symmetric stretching vibration, and phenolic alcohol associated hydroxyl groups; stage IV and full-stage showed consistency with stage II. In stage V, the three functional groups with the greatest correlation were the methyl asymmetric stretching vibration, benzene ring, and -COOH. Among them, the correlation coefficient of the benzene ring from stage IV to stage V was 0.932–0.993, indicating a strong positive correlation of aromatic C=C at high temperatures, which indicates structural stabilization. This is because the more aromatic the hydrocarbons, the tighter the structure of the coal. Additionally, the C=O and C–O–C groups reached their maximum correlation coefficients in Stage V during the stage evolution, with values of −0.95 and −0.953, respectively. This indicates that the functional groups with the strongest negative correlation shifted from aliphatic hydrocarbons to oxygen-containing groups over the course of pyrolysis. These groups are rapidly consumed at high temperatures, releasing gaseous products, including hydrogen, and facilitating the formation of porous coke, resulting in a sharp decline in the coal mass and a rapid increase in the conversion rate. In summary, aliphatic hydrocarbons maintain a high correlation throughout the entire oxygen-free pyrolysis process of gas coal, dominating the increase in the mass conversion rate. However, during the later stages of oxygen-free pyrolysis, the high correlation of oxygen-containing functional groups and aromatic hydrocarbons gradually overshadows the contribution of aliphatic structures. This phenomenon primarily arises from the cleavage of long-chain aliphatic hydrocarbons into shorter-chain fragments during coal oxygen-free pyrolysis, followed by aromatization reactions that convert these chain hydrocarbons into structurally stable polycyclic aromatic hydrocarbons, which subsequently undergo condensation reactions.

3.3. Differences in the evolution of active functional groups influenced by coal rank

To clarify the impact of coal rank on the real-time evolution laws of functional groups in gas coal, this section analyzes the real-time evolution of functional groups during the oxygen-free pyrolysis of long-flame coal and lignite, revealing the differences in the evolution of functional groups under the influence of coal rank. The information on the coal samples is consistent with data published in a previous study (Xin et al., 2024a). Fig. 9 shows the three-dimensional real-time infrared spectra of long-flame coal and lignite during oxygen-free pyrolysis at a heating rate of 2 °C/min. Fig. 10 illustrates the baseline drift correction process using -CH_3 as an example, revealing that, compared to gas coal, the baseline drift significantly impacts the overall variation pattern of -CH_3 in lignite. The actual intensity variation pattern of -CH_3 in coal is characterized by initially remaining unchanged and then rapidly decreasing after a certain temperature, while the uncorrected curve variation pattern of -CH_3 shows a slow increase followed by a rapid increase. This discrepancy is primarily caused by the baseline drift toward higher intensities with increasing temperature.

Fig. 11 shows the baseline-corrected real-time infrared evolution curves. Combined with Fig. 7, it is evident that the consumption or generation trends of functional groups across the different coal types are broadly similar. However, variations in coal rank lead to distinct differences in group distribution, structural characteristics, and extent/timing of group consumption or generation. The lower the rank of coal, the less significant is the consumption of aliphatic hydrocarbons in the early period of oxygen-free pyrolysis, with the volatile initial release

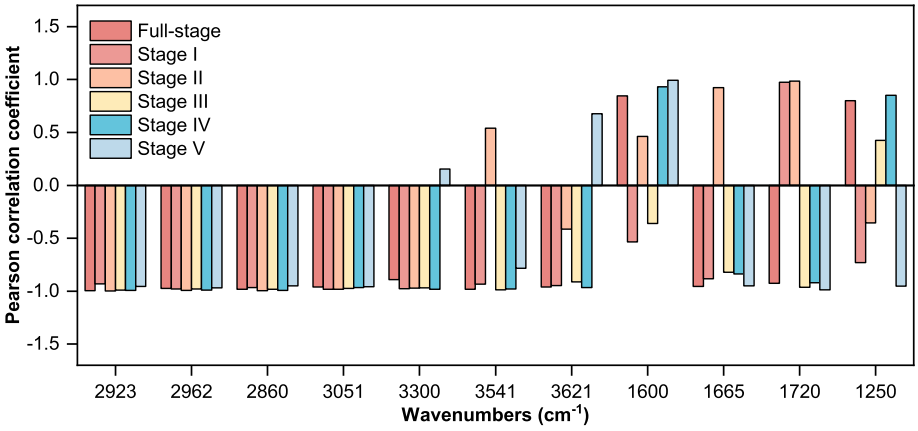

Fig. 8. Pearson correlation coefficients between microstructure and conversion rate.

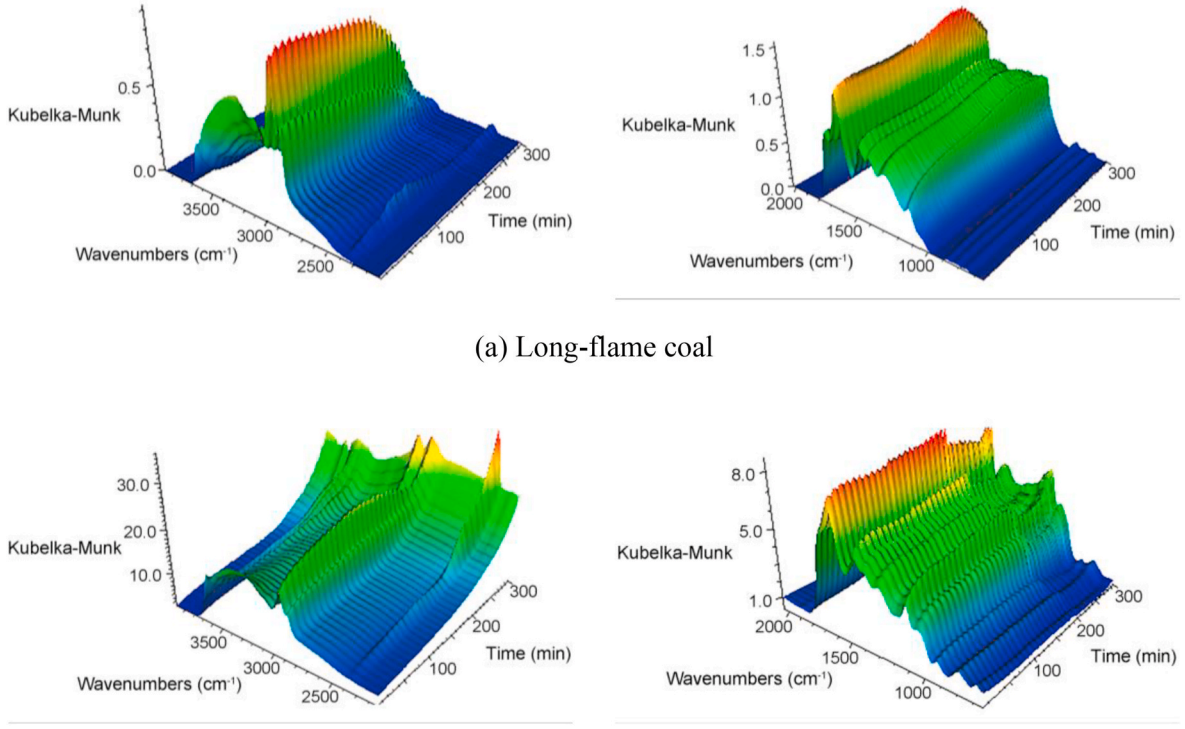

Fig. 9. 3D real-time infrared spectra during oxygen-free pyrolysis.

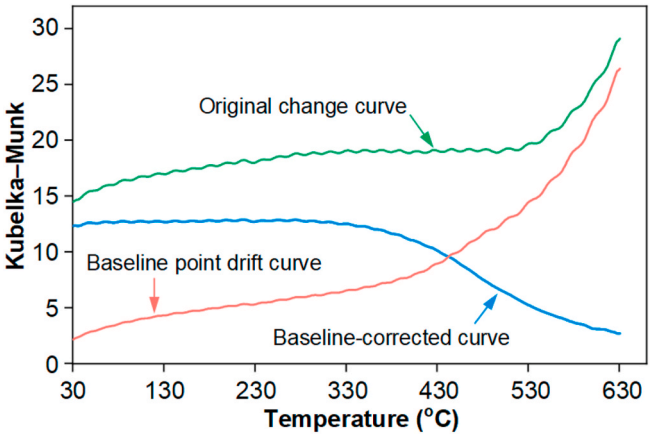

Fig. 10. Baseline drift correction of lignite with temperature (using -CH_3 as an example).

point increasingly reliant on the reduction of oxygen-containing functional groups. In other words, the volatile initial release in lignite is mainly due to the breaking of chemical bonds with weak forces, such as oxygen-containing groups in coal, and the formation of more small-molecular structural fragments that are easy to volatilize. This underscores the oxygen-containing functional groups as the triggering mechanism for coal oxygen-free pyrolysis, a conclusion aligned with the findings from Pearson correlation analyses. Conversely, although the degree of coalization increases, gas coal with a high volatile content still retains relatively abundant aliphatic bridge bonds, thereby enhancing molecular structural stability and requiring higher energy to cleave these bonds during oxygen-free pyrolysis. Therefore, with the increase in coal rank, the role of aliphatic hydrocarbons in the release of the volatile content of coal begins to increase, resulting in a higher initial release-point temperature of the volatile content. At the later stage of thermal decomposition, the rapid decomposition of colloidal bodies and the formation of semi-coke accelerated the rapid reduction of aliphatic hydrocarbons, oxygen-containing functional groups, hydroxyl groups, and aromatic hydrocarbons in coal.

To further clarify the impact of coal rank on the evolution of functional groups in gas coal, the differences in infrared curves among coal types were analyzed by establishing characteristic transition parameters, such as the onset temperature of rapid consumption, maximum consumption rate, and maximum consumption rate point temperature. The onset temperature of rapid consumption refers to the inflection point temperature at which the infrared curve transitions from a slow to a rapid decline. The maximum consumption rate is defined as the maximum value of the first derivative of the KM function with respect to temperature, typically observed during the later stages of oxygen-free pyrolysis, and the maximum consumption rate point temperature corresponds to the temperature at this maximum rate. Taking the methyl asymmetric stretching vibration in aliphatic hydrocarbons as an example, Fig. 12 illustrates the extraction method for these characteristic transition parameters.

Based on Figs. 7 and 11, combined with the parameter extraction method in Fig. 12, it was observed that during the entire oxygen-free pyrolysis process, lower coal ranks correlated with increased infrared intensity values for all functional groups and increasingly distinct characteristic transition points for their rapid decrease. Specifically, for aliphatic hydrocarbons, the onset temperature of rapid consumption decreased with decreasing coal rank, the maximum consumption rate increased with lower coal ranks, and the maximum consumption rate point temperature remained largely unaffected by the coal rank. For example, the onset temperature of rapid consumption for methyl asymmetric stretching vibration increased from 357.1 °C in lignite to 386.7 °C in long-flame coal and 414.8 °C in gas coal, representing

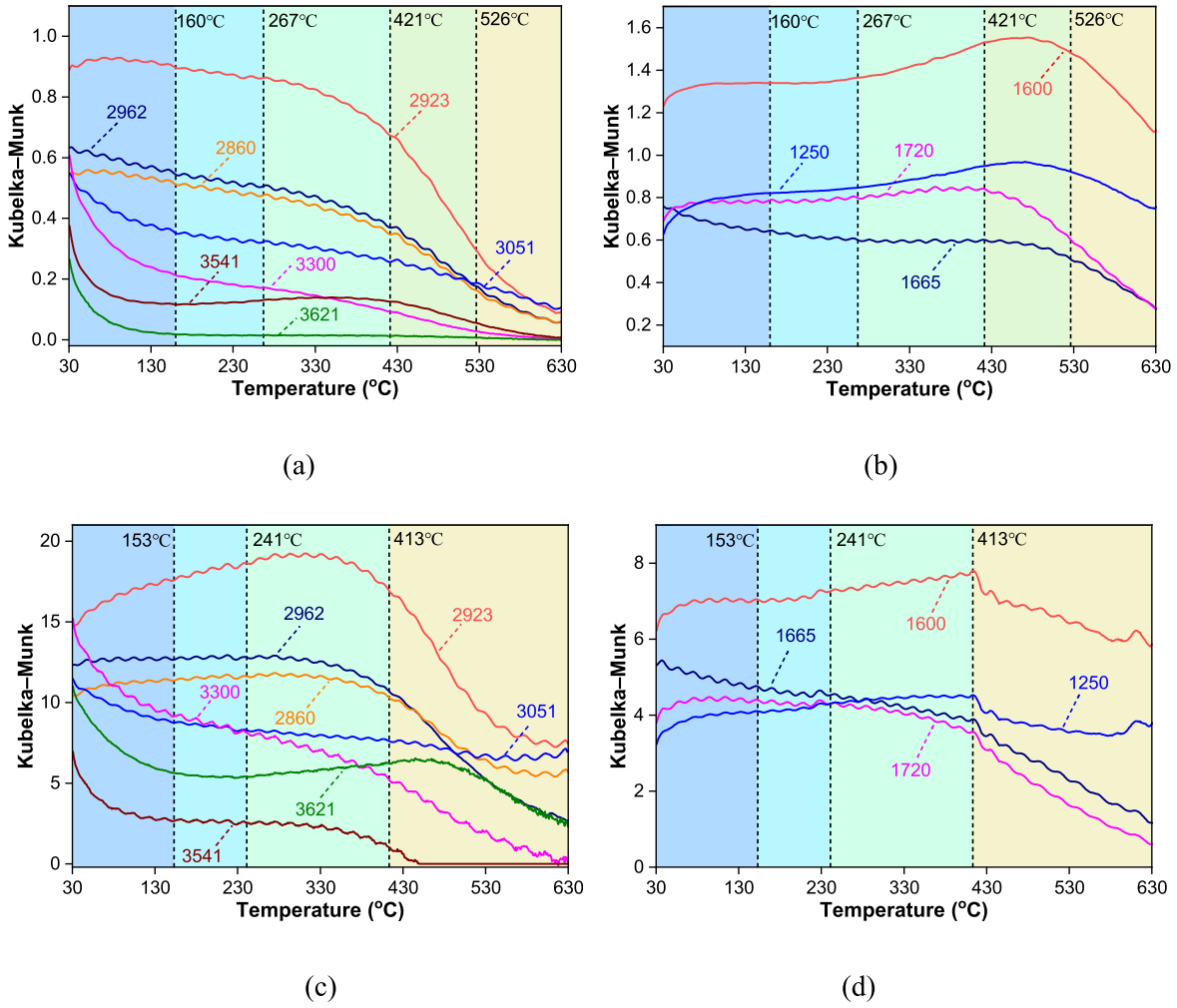

Fig. 11. Real-time evolution curves of functional groups during oxygen-free pyrolysis (a and b: long-flame coal; c and d: lignite).

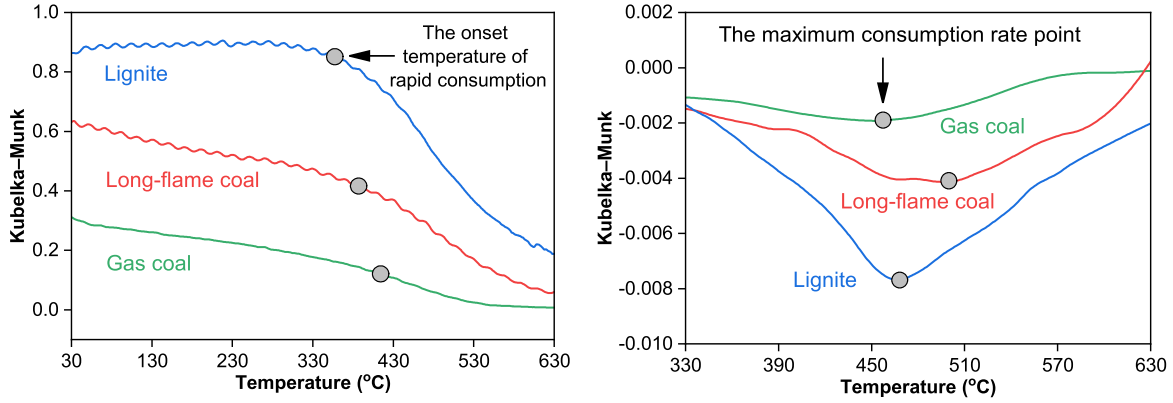

Fig. 12. Schematic diagram of the extraction of characteristic transition parameters.

increases of 8.3 % and 16.2 %, respectively. The maximum consumption rate increased from −0.0019 for gas coal to −0.0041 for long-flame coal and −0.0077 for lignite (the negative sign indicates the direction of change). The C=O and -COOH groups are affected by the coal rank in a law that is basically the same as that of aliphatic hydrocarbons. As coal rank decreases, benzene ring consumption becomes more pronounced in the later stages of oxygen-free pyrolysis, with the onset temperature of rapid benzene ring consumption in lignite shifting to 414 °C, while gas coal exhibits no benzene ring depletion before oxygen-free pyrolysis concludes, a phenomenon governed by the degree of coalification. The Ar-CH groups show a consistent decline across coal ranks, unaffected by coal rank. Additionally, the C-O-C bonds in the different coals exhibited a certain degree of increase. With an increase in temperature, a large number of chain breaks occurred in C-O-C, which was easy to break, and it began to decrease continuously. Meanwhile, lower coal ranks corresponded to an earlier onset temperature of the rapid consumption in C-

O-C, decreasing from 600.0 °C in gas coal to 473.6 °C in long-flame coal and 413.1 °C in lignite. In gas coal, hydroxyl groups are nearly fully depleted during oxygen-free pyrolysis, whereas lignite retains thermally stable hydroxyls, predominantly free hydroxyls, indicating that hydroxyl stability increases with decreasing coal rank. Notably, compared to high-rank gas coal, pyrolyzed lignite has not been widely utilized (Ahmed and Gupta, 2013). Therefore, these findings on the influence of coal rank on gas coal provide critical insights for advancing large-scale, high-quality, and comprehensive utilization of low-rank coals.

3.4. Differences in the evolution of active functional groups influenced by time-scale effects

To elucidate the impact of time-scale effects on the real-time evolution of functional groups during oxygen-free pyrolysis of gas coal, this section reveals the differential mechanisms of active group reactions under the influence of time-scale effects through comparative analysis of the evolutionary laws of functional groups at heating rates of 2, 5, and 10 °C/min. Notably, owing to the thermal effects of gas coal and its inherent ash structure, abrupt spectral changes occur in oxygen-containing functional groups (within the 2000–400 cm^{-1} wavenumber range) after 430 °C. Therefore, the oxygen-containing functional groups were excluded from the analysis here. Fig. 13 displays the 3D infrared spectra within the wavenumber range of 4000–2050 cm^{-1}. After two-step baseline drift correction, the evolution curves of the functional groups during the oxygen-free pyrolysis of gas coal under different heating rates were obtained, as shown in Fig. 14.

By comparing Figs. 7 and 14 from the perspective of functional group consumption, it is evident that lower heating rates prolong the actual duration of oxygen-free pyrolysis at each temperature, but do not alter the overall evolutionary trends of functional groups. The oxygen-free pyrolysis process of coal takes thermal decomposition as the main process, and the decomposition of various groups has a clear bond breaking process. Thermal decomposition of coal primarily occurs in medium-to-high temperature ranges, and the process is rapid. The cumulative effect on time manifests as delays in the onset temperature of rapid consumption, maximum consumption rate point temperature, and onset temperature of rapid increase in the benzene ring (i.e., the inflection point where equilibrium transitions to rapid increase) with increasing heating rates. Especially, aliphatic hydrocarbons exhibited pronounced time-scale effects when the heating rate increased from 2 °C/min to 5 °C/min, whereas benzene rings showed significant time-scale effects when the heating rate increased from 5 °C/min to 10 °C/min. The hydroxyl groups clearly demonstrate time-scale effects, as both the onset temperature of rapid consumption and the maximum consumption rate point temperature are delayed with higher heating rates. However, the functional groups exhibited distinct initial infrared intensity values under different heating rates. Although these differences do not affect the analysis of the aforementioned characteristic transition parameters, they introduce variability when evaluating the impact of the time-scale effects on the overall reaction processes of the functional groups. Therefore, to further clarify the influence of time-scale effects on the global reaction of functional groups, the conversion rates of active functional groups during the oxygen-free pyrolysis of gas coal at different heating rates were calculated, as illustrated in Fig. 15.

As shown in Fig. 15, the conversion rate of the methyl asymmetric stretching vibration is significantly delayed to higher temperatures with increasing heating rates after 445 °C, which is manifested as a lower conversion rate of the group at the same temperature, and the cumulative effect of time is considered to be obvious here. Prior to 445 °C, however, the conversion rate of the methyl asymmetric stretching vibration remained largely unaffected by time-scale effects. Similarly, the conversion rate of the methylene asymmetric stretching vibration was delayed after 415 °C as heating rate increased. The methylene symmetric stretching vibration, Ar-CH groups, water associated hydroxyl groups, and phenolic alcohol associated hydroxyl groups exhibited marked time-scale effects after 450 °C, 490 °C, 430 °C, and 370 °C, respectively. The benzene rings and free hydroxyl groups showed analogous behavior, with their conversion rate curves during the later stages of oxygen-free pyrolysis being notably delayed under heating rate changed from 2 °C/min (or 5 °C/min) to 10 °C/min. Specifically, the key transition temperature points for benzene rings shift significantly due to time-scale effects—from 440 °C to 459 °C and then to 557 °C as heating rates increase, corresponding to delays of 19 °C between 2 °C/min and 5 °C/min, and 98 °C between 5 °C/min and 10 °C/min. Similarly, the key transition temperature points for free hydroxyl groups were delayed by 68 °C and 86 °C for the same heating rate intervals. These results indicate that the key transition temperature points of the benzene rings and free hydroxyl groups exhibit high sensitivity to the time-scale effects of the change in the high heating rate. Consequently, the conversion rates of active functional groups in gas coal during the early stages of oxygen-free pyrolysis remain largely unaffected by time-scale effects. In contrast, during the later stages, the accumulated effects of the time-scale result in a shift of conversion rates toward higher temperatures. These phenomena are primarily attributed to the fact that, at low temperatures, the reactions mainly involve the breaking of weak bonds. The coal matrix has not yet undergone large-scale pyrolysis and the pore structure remains largely unchanged. The generated volatile small molecules can diffuse relatively easily. Therefore, although increasing the heating rate shortens the reaction time, it also increases the rate of the energy input. The effects of these two factors on the reaction process counteract each other to a certain extent. In contrast, the greater sensitivity to the heating rate at high temperatures is fundamentally due to the depolymerization and reorganization of the macromolecular network structures. These reactions inherently require high activation energies. Under high heating rates, a heat transfer lag occurs, resulting in significant temperature differences that greatly influence the reaction rate, thereby governing the consumption of functional groups within the coal particles.

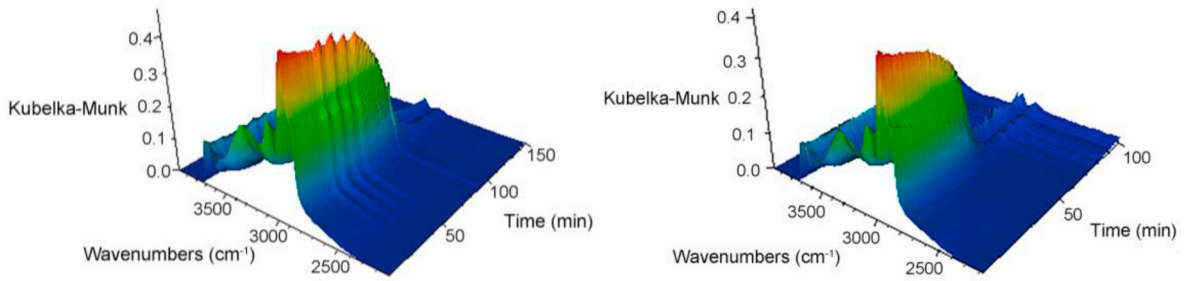

Fig. 13. 3D real-time infrared spectra of gas coal during oxygen-free pyrolysis.

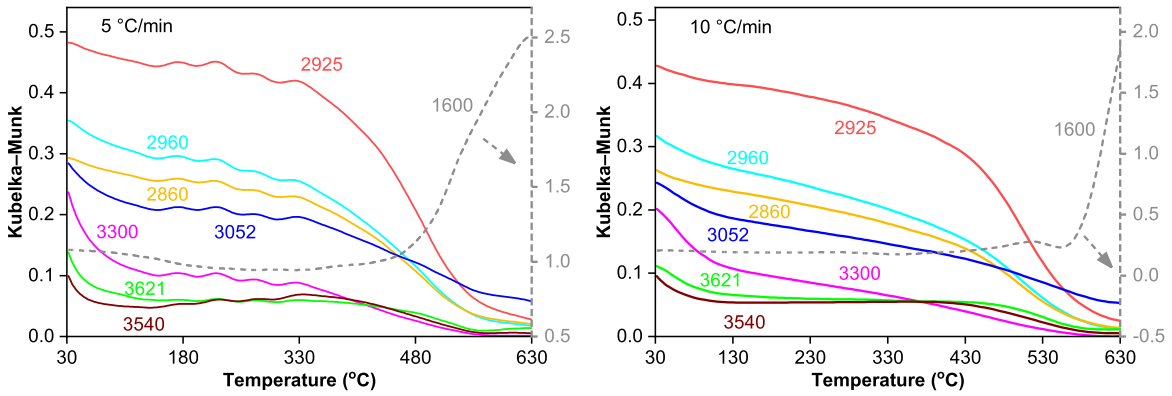

Fig. 14. Evolutionary curves of functional groups during oxygen-free pyrolysis of gas coal at different heating rates.

3.5. Kinetic analysis of functional group reactions during oxygen-free pyrolysis of gas coal

According to the transformation process of the oxygen-free pyrolysis groups of gas coal, it can be concluded that aliphatic hydrocarbons and Ar-CH groups contribute more to the oxygen-free pyrolysis of coal in the early stage, whereas oxygen-containing groups contribute more to the oxygen-free pyrolysis in the later stage. This is because oxygen-containing groups are mainly derived from aliphatic hydrocarbons and Ar-CH groups in the early stage of oxygen-free pyrolysis. In later stages, owing to the continuous depletion of aliphatic hydrocarbons and Ar-CH, their contribution gradually decreased, shifting to the consumption of oxygen-containing groups. Therefore, to elucidate the kinetic mechanisms of the functional group reactions during oxygen-free pyrolysis, the Coats-Redfern model was employed to calculate the kinetic parameters for aliphatic hydrocarbons and Ar-CH groups throughout the entire process. However, global fitting yielded unsatisfactory results, whereas stage-wise fitting (divided by the onset temperature of rapid consumption) yielded superior performance. Before 85 °C, it was mainly the rapid drying and degassing stage, so no analysis was performed. For the oxygen-containing functional groups and hydroxyl groups, the kinetics of their later consumption processes were mainly calculated; for the benzene ring bonds, the kinetics of the rising phase of the curve were mainly calculated. Notably, the kinetic calculations exhibit a better fitting performance for monotonic upward or downward trends. Therefore, the rising and falling stages of the C-O-C groups were independently calculated. The KM conversion rates of different functional groups were incorporated into 21 different reaction mechanism functions, and linear regression equations for each functional group were derived through inverse calculations. Fig. 16 illustrates the fitting curves for aliphatic hydrocarbons as an example, and Table 5 summarizes the kinetic parameters of the different groups under the best-fit conditions.

According to the calculation results in Table 5, the average activation energy ($\overline{E_a}$) during the oxygen-free pyrolysis of gas coal follows the order C-O-C > benzene rings > aliphatic hydrocarbons > carboxyl groups > carbonyl groups > hydroxyl groups. However, during oxygen-free pyrolysis, the apparent activation energy depends not only on the difficulty of the initial bond cleavage (bond energy), but also on the efficiency of subsequent chain reactions triggered by that cleavage. If a functional group generates highly active free radicals through low-bond-energy cleavage and efficiently propagates through the reaction chain, the overall apparent activation energy of the process is low. Conversely, a higher activation energy was observed. Specifically, the E_a values of aliphatic hydrocarbons and Ar-CH groups in the early stages of oxygen-free pyrolysis were significantly lower than those in the later stages. For example, the E_a for methyl asymmetric stretching vibration is 41.0 kJ/mol in the temperature range of 85–390 °C, but increases to 165.6 kJ/mol at 390–630 °C. This indicates that at lower temperatures, consumption primarily involves methyl and methylene groups in the long alkyl side chains or aliphatic bridge structures attached to the edges of the coal matrix. After the depletion of these less stable long alkyl chains, reactions at higher temperatures require the cleavage of methyl or methylene groups directly linked to aromatic rings. The aromatic ring is a strong electron withdrawing group. When methyl or methylene groups are directly attached, the electron cloud of the carbon atom is drawn toward the ring, significantly strengthening the C-H bond energy. Thus, at elevated temperatures, the reaction shifts from cleaving "weak" aliphatic bonds to breaking "strong" aryl-aliphatic bonds. A substantial difference in the bond energy directly leads to a sharp increase in the apparent activation energy. The reaction mechanism for aliphatic hydrocarbons is $\left[1-(1-\alpha)^{1/3}\right]^2$, representing random nucleation and nucleus growth (Avrami-Erofeev model, n = 4). This suggests that their decomposition does not proceed uniformly but begins with the cleavage of weak bonds distributed randomly in the structure (nucleation), which subsequently triggers the rapid dissociation and volatilization of adjacent alkyl chains, consistent with the characteristics of free radical chain reactions. The E_a for Ar-CH increases from 7.3 kJ/mol to 27.1 kJ/mol. Although the absolute values were much lower than those of aliphatic hydrocarbons, the underlying reason for the increasing trend was the same. The mechanism function for Ar-CH is $1-2\alpha/3-(1-\alpha)^{2/3}$, representing a diffusion model. The reaction rate was likely limited by the desorption and diffusion of H radicals from the surface or edges of the aromatic layers. Throughout the oxygen-free pyrolysis process, the E_a for benzene rings was 269.6 kJ/mol. This is because the later stages of oxygen-free pyrolysis involve the transformation of the coal structure into semi-coke or char, a process essentially comprising dehydrogenation and cross-linking reactions between the highly condensed aromatic structures. These reactions require direct cleavage of the stable C-C bonds within the aromatic rings, which have a very high bond energy (518 kJ/mol) (Zhu et al., 2024), making this one of the most energy-intensive steps in pyrolysis. The mechanism function for the benzene rings is $-ln(1-\alpha)$, representing a first-order chemical reaction. This indicates that the decomposition rate is directly proportional to the concentration of unreacted benzene rings, constituting a homogeneous, deep pyrolysis process that requires substantial energy input. The activation energy of the water associated hydroxyl groups increased with increasing temperature. The reaction mechanism function is $\left[1-(1-\alpha)^{1/3}\right]^2$, which corresponds to a three-dimensional diffusion-controlled condensation reaction. This suggests that in the low-temperature region, the reaction is primarily dominated by the breaking and reorganization of hydrogen bond networks with a lower energy barrier. In the high-temperature region, more intense hydroxyl condensation dehydration reactions may occur, requiring overcoming the energy barriers associated with covalent bond reorganization and intramolecular diffusion. It is noteworthy that among all

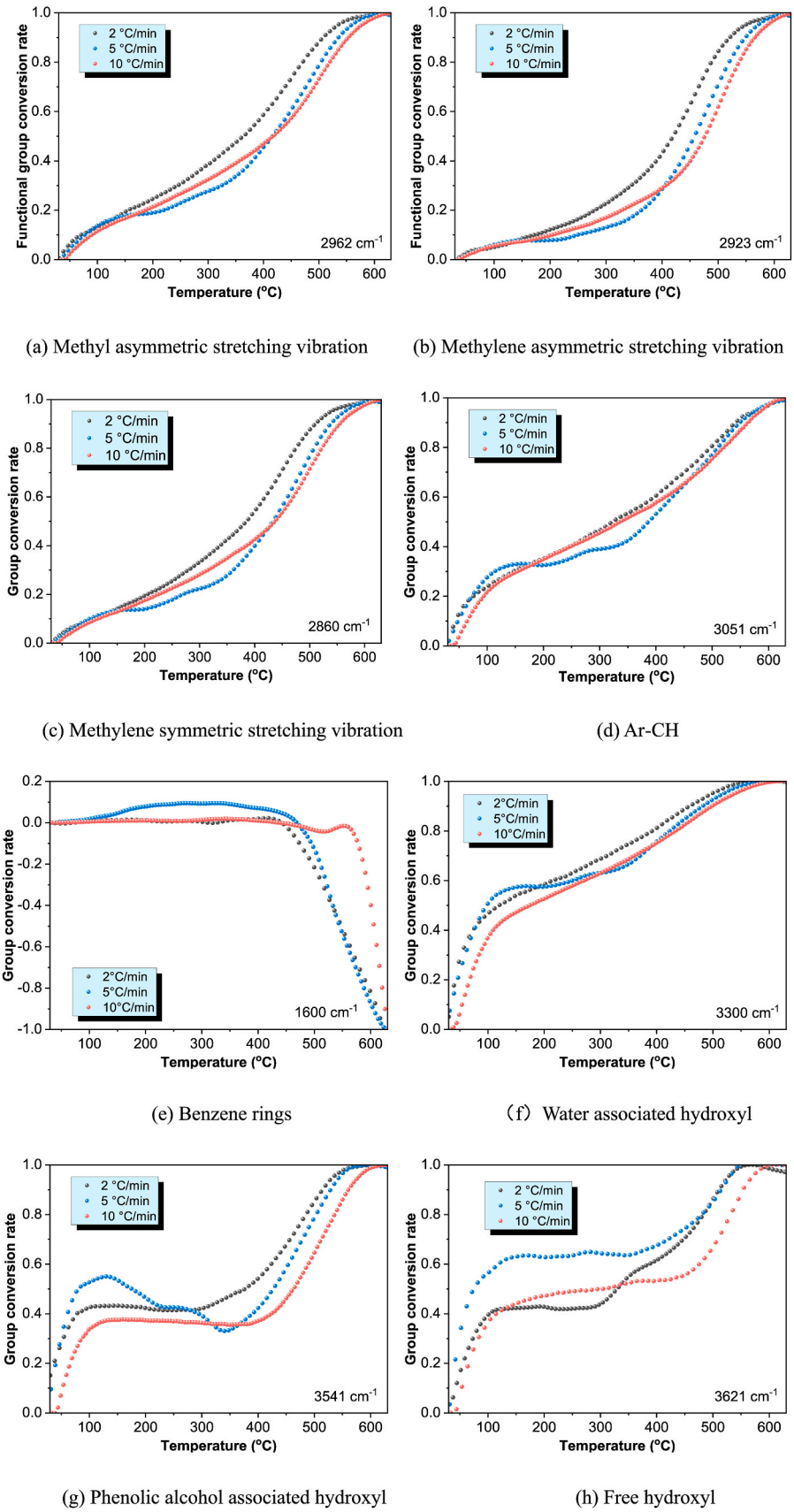

(a) Methyl asymmetric stretching vibration (b) Methylene asymmetric stretching vibration

(c) Methylene symmetric stretching vibration (d) Ar-CH

(e) Benzene rings (f) Water associated hydroxyl

(g) Phenolic alcohol associated hydroxyl (h) Free hydroxyl

Fig. 15. Conversion rates of active functional groups during oxygen-free pyrolysis of gas coal at different heating rates.

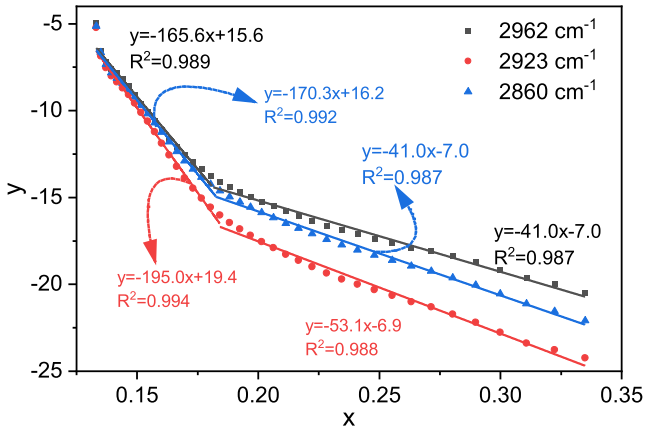

Fig. 16. Fitting curves for aliphatic hydrocarbons during oxygen-free pyrolysis of gas coal.

Table 5
Kinetic fitting parameters for oxygen-free pyrolysis of gas coal.

Group	Fitting temp (°C)	Fitting equation	R^2	E_a/(kJ/mol)	$\overline{E_a}$/(kJ/mol)	$g(\alpha)$
2962	85–390	y = −41.0x-7.0	0.987	41.0	103.3	$g(\alpha)$
	390–630	y = −165.6x+15.6	0.989	165.6		21
2923	85–380	y = −53.1x-6.9	0.988	53.1	124.1	
	380–630	y = −195.0x+19.4	0.994	195.0		
2860	85–385	y = −48.3x-6.1	0.992	48.3	109.3	
	385–630	y = −170.3x+16.2	0.992	170.3		
3051	85–430	y = −7.3x-14.7	0.976	7.3	17.2	$g(\alpha)$
	430–630	y = −27.1x-11.2	0.993	27.1		10
1600	444–630	y = −269.6x+25.1	0.936	269.6	269.6	$g(\alpha)$ 1
3300	85–210	y = −3.4x-14.4	0.869	3.4	13.3	$g(\alpha)$
	210–390	y = −5.8x-13.9	0.948	5.8		9
	390–567	y = −30.8x-9.4	0.961	30.8		
3541	316–556	y = −27.8x-9.4	0.963	27.8	27.8	$g(\alpha)$
3627	310–563	y = −13.8x-11.5	0.944	13.8	13.8	7
1665	320–630	y = −46.2x-7.5	0.974	46.2	46.2	
1720	308–630	y = −65.2x-4.9	0.972	65.2	65.2	
1250	432–596	y = −168.2x+11.0	0.964	168.2	253.4	$g(\alpha)$ 1
	596–630	y = −338.6x+32.0	0.963	338.6		$g(\alpha)$ 18

oxygen-containing functional groups, hydroxyl groups exhibit the lowest activation energy. This is because their reaction initiates via cleavage of the C-O bond in aliphatic alcohols or homolytic cleavage of the O-H bond (as represented by chain reactions R1–R2 in Fig. 17), generating highly active free radicals such as H• and •OH (or Ph-CH_2•). These radicals rapidly propagate the reaction chain through efficient hydrogen abstraction reactions (R3–R4), continuously generating new free radicals. As a result, the high energy input required initially is distributed across the entire rapidly developing chain reaction, leading to a low apparent activation energy for the overall process. In contrast, the consumption of carbonyl groups requires the cleavage of the α-C-C bond (R5), and the consumption of carboxyl groups requires decarboxylation involving the cleavage of C-C or O-H bonds (R7–R8). Although some of these bond energies are slightly lower than those of the O-H bond (Li et al., 2015; Ruscic et al., 2002; Shen and Fang, 2011), their key reaction pathways often produce stable products or intermediates, such as H_2O (R10), CH_4 (R6), CO_2 (R9), or Ph-CO• (R5 and R8). The latter, owing to conjugation effects, is extremely stable and tends to terminate rather than propagate the reaction chain. Consequently, the efficiency of the subsequent chain reactions is relatively low, manifesting as a higher apparent activation energy. The mechanism function for C=O and -COOH is α^2, representing a diffusion model. This indicates that the higher activation energy of carboxyl and carbonyl groups stems not only from their bond cleavage and chain termination tendencies but is also closely related to the physical mechanism of their reactions being diffusion-controlled. For instance, the formation and release of CO_2 gas molecules from carboxyl groups within the pores of coal particles may be the rate-determining step. Interestingly, although aliphatic hydrocarbons undergo more extensive consumption than oxygen-containing functional groups, their activation energy in the high-temperature region is higher than that of the carboxyl and carbonyl groups. This was primarily due to the dynamic balance between the formation and consumption of oxygen-containing functional groups (especially C=O) during pyrolysis. A large number of radical intermediates generated in the initial stages of aliphatic hydrocarbon decomposition can attack the coal matrix, leading to the formation of new oxygen-containing functional groups in certain carbon structures. Consequently, the net consumption rate of oxygen-containing functional groups appears slower, and their concentration exhibits a plateau during specific stages, thereby kinetically manifesting a relatively stable low-consumption state and a lower apparent activation energy. For C-O-C bonds, the activation energy during the rapid increase stage is 168.2 kJ/mol, with a mechanism function of $-ln(1-\alpha)$, representing a first-order chemical reaction. This stage primarily involves the cleavage of aliphatic-aromatic ether bonds (Ph-O-R) with lower bond energy (R12). In contrast, during the rapid decrease stage, the activation energy surges to 338.6 kJ/mol, and the kinetics shift to the Avrami-Erofeev model (n = 1/3). This signifies that the reaction targets the residual ether bonds in the later stages of coal carbonization, which have very high bond energy, such as diaryl ether bonds (Ph-O-Ph') (R13). The value n = 1/3 often indicates a nucleation and growth process limited by diffusion, indicating that ether bond cleavage no longer occurs uniformly but is confined to interfaces or defect sites within a highly cross-linked, graphitized aromatic cluster network. The reaction process requires overcoming both high chemical bond energy and significant mass transfer resistance. This analysis provides critical insights into understanding the essence of the complex network reactions during coal oxygen-free pyrolysis.

3.6. Industrial implications

This study employed in situ FTIR to investigate the evolution of functional groups during the oxygen-free pyrolysis of coal and analyzed the kinetics of the functional group reactions. These findings provide a theoretical foundation for the development of clean and efficient utilization technologies for low-rank coal1. Specifically, for the potential technology of in situ underground coal pyrolysis, the design of pyrolysis processes for low-rank coal should focus on operating conditions within the decomposition range of oxygen-containing functional groups to efficiently handle volatile release. In contrast, for high-rank coal, attention should be directed toward the decomposition range of aliphatic hydrocarbons. Furthermore, the evolution of the functional groups offers valuable insights into the purification of products from low-temperature pyrolysis. For instance, eliminating Ph-COO• radicals can reduce CO_2 emissions, whereas enhancing the hydrogen abstraction capability of CH_3• radicals can effectively promote CH_4 extraction. These strategies contribute to improving coal utilization efficiency and reducing environmental pollution. Additionally, the times-cale effects primarily influence the later stages of oxygen-free coal pyrolysis, underscoring its significance for the rapid regulation and production of semi-coke.

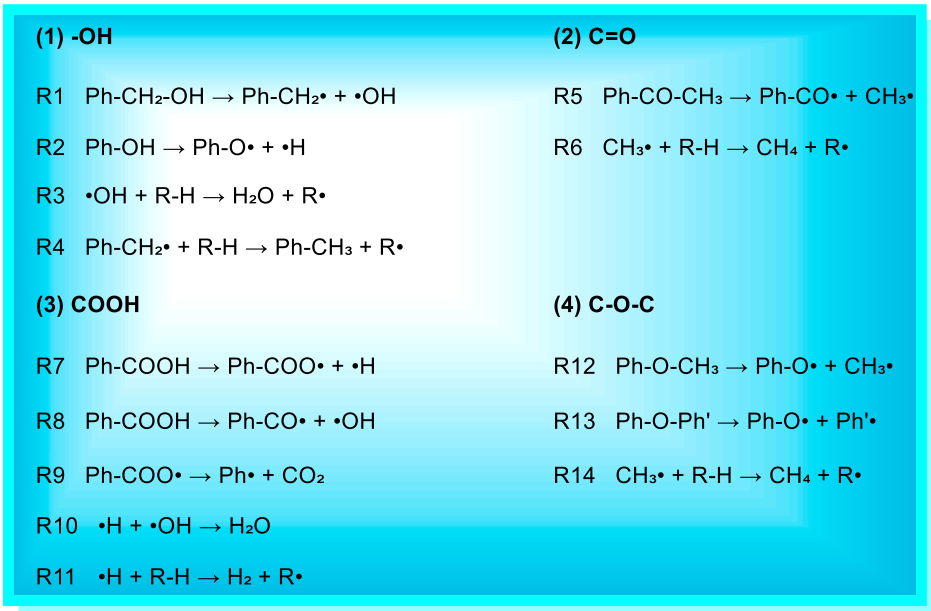

Fig. 17. Schematic diagram of the chain reaction initiated by cleavage of hydroxyl and oxygen-containing groups.

4. Conclusion

Based on the research findings, the following conclusions can be drawn:

(1) Among the 11 types of functional groups, oxygen-containing groups accounted for the highest proportion of gas coal. Across different stages, aliphatic hydrocarbons maintain a strong correlation with the mass loss conversion rate, while in the later stages (Stages IV-V), this high correlation transitions to being predominantly associated with oxygen-containing functional groups and aromatic hydrocarbons. With a decreasing coal rank, the initial release of volatiles relies more heavily on the consumption of oxygen-containing groups. With increasing coal rank, the role of aliphatic hydrocarbons in elevating the volatile initial release temperature intensifies. These findings confirm that oxygen-containing functional groups act as the triggering mechanism for coal oxygen-free pyrolysis.

(2) Gas coal is significantly influenced by coal rank and time-scale effects: with decreasing coal rank, the onset temperature of rapid consumption for all functional groups during the later stages of oxygen-free pyrolysis advances, the maximum consumption rate of aliphatic hydrocarbons increases, and the stability of hydroxyl groups is enhanced. Time-scale effects predominantly impact the later stages of oxygen-free pyrolysis in gas coal. As the heating rate increased, the characteristic temperatures (e.g., the onset temperature of rapid consumption) and functional group conversion rates shifted toward higher temperatures. This indicates that the time-scale effect is governed by the high activation energy at elevated temperatures and the heat transfer hysteresis.

(3) During the oxygen-free pyrolysis of gas coal, the average activation energy followed the order C-O-C > benzene rings > aliphatic hydrocarbons > carboxyl groups > carbonyl groups > hydroxyl groups. The magnitude of the apparent activation energy primarily depends on the difficulty of the initial bond cleavage and the efficiency of the subsequent chain reactions. The activation energy of C-O-C increases from 168.2 kJ/mol to 338.6 kJ/mol with rising temperature, reflecting the formation of higher bond energy (e.g., Ph-O-Ph'). The high activation energy of the benzene rings (269.6 kJ/mol) indicates the development of structural skeletons in semi-coke or char. The activation energy of aliphatic hydrocarbons at high-temperature stages was greater than that at low-temperature stages. The reaction mechanism of aliphatic hydrocarbons is governed by random nucleation and nucleus growth, whereas oxygen-containing functional groups and Ar-CH groups are controlled by diffusion models.

(4) In future work, a combined approach of thermogravimetry-infrared spectroscopy-gas chromatography-mass spectrometry (TG-FTIR-GC-MS) coupled with molecular dynamics simulations will be employed to investigate the synergistic mechanisms between oxygen-free pyrolysis products and free radical chain reactions in low-rank coal.

CRediT authorship contribution statement

Guangyu Bai: Writing – original draft, Methodology, Investigation, Funding acquisition. **Haihui Xin:** Writing – review & editing, Supervision, Conceptualization. **Pengcheng Zhang:** Formal analysis. **Chao Luo:** Investigation. **Jinliang Li:** Resources. **Qiang Zeng:** Investigation. **Bekir Genc:** Supervision. **Moshood Onifade:** Supervision. **Deming Wang:** Conceptualization.

Declaration of competing interest

The authors declare that they have no known competing financial interests or personal relationships that could have appeared to influence the work reported in this paper.

Acknowledgments

This work was funded by the Graduate Innovation Program of China University of Mining and Technology (Grant No. 2024WLKXJ155), "the Fundamental Research Funds for the Central Universities" (Grant No. 2024-10982), and the Postgraduate Research & Practice Innovation Program of Jiangsu Province (Grant No. KYCX24_2928).

Data availability

The data that has been used is confidential.

References

Ahmed, I., Gupta, A., 2013. Experiments and stochastic simulations of lignite coal during pyrolysis and gasification. Appl. Energy 102, 355–363.

Aprianti, N., Faizal, M., Said, M., Nasir, S., Fudholi, A., 2023. Gasification kinetic and thermodynamic parameters of fine coal using thermogravimetric analysis. Energy 268, 126666.

Bai, G., Xin, H., Yang, Y., Li, J., Qi, X., Zhang, P., Wang, J., Liu, J., Ma, L., 2025. Stage development characteristics of oxygen-lean combustion of coal in fire zone. Part I: the evolution law of pyrolysis and combustion stage characteristics. J. Therm. Anal. Calorim. 150 (1), 327–343.

Bai, G., Xin, H., Zhang, P., Yang, Y., Wang, D., Qi, X., Wu, Z., Huang, Y., 2024. Fire zone forefront residual tar combustion characteristics and functional group transformation mechanism: appling the based on thermogravimetric and in-situ high-temperature FTIR. Appl. Therm. Eng. 249, 123404.

Cai, Y., Zhai, C., Yu, X., Sun, Y., Xu, J., Zheng, Y., Cong, Y., Li, Y., Chen, A., Xu, H., 2023. Quantitative characterization of water transport and wetting patterns in coal using LF-NMR and FTIR techniques. Fuel 350, 128790.

Çepelioğullar, Ö., Haykırı-Açma, H., Yaman, S., 2016. Kinetic modelling of RDF pyrolysis: model-fitting and model-free approaches. Waste Manag. 48, 275–284.

Coats, A.W., Redfern, J., 1964. Kinetic parameters from thermogravimetric data. Nature 201 (4914), 68–69.

Dai, F., Zhuang, Q., Huang, G., Deng, H., Zhang, X., 2023. Infrared spectrum characteristics and quantification of OH groups in coal. ACS Omega 8 (19), 17064–17076.

Deng, Y., Wang, C.-P., Xiao, Y., Chen, H.-L., Deng, J., Du, Y.-X., Bai, G.-X., 2023. Effect of greenhouse gases emissions from coal spontaneous combustion under different inerting conditions in the quenching process. J. Therm. Anal. Calorim. 148 (11), 4883–4895.

Gopinathan, P., Subramani, T., Barbosa, S., Yuvaraj, D., 2023. Environmental impact and health risk assessment due to coal mining and utilization. Environ. Geochem. Health 45 (10), 6915–6922.

Hameed, Z., Khan, Z., Khurram, S., Inayat, A., Amin, N., Aslam, M., Watson, I., 2024. Co-gasification study of blends of municipal solid waste with sugarcane bagasse and rice husk using the coats-redfern method. J. Energy Inst. 113, 101542.

Hu, R.-z., Shi, Q.Z., 2008. Thermal Analysis Kinetics.

Hu, R., Chen, S., Gao, S., Zhao, F., Luo, Y., Gao, H., Shi, Q., Zhao, H., Yao, P., Li, J., 2005. Thermal decomposition kinetics of the Pb0. 25Ba0. 75 (TNR)· H2O complex. J. Hazard Mater. 117 (2–3), 103–110.

Huang, F., Zou, J., Lan, W., Zhou, J., Fang, H., 2025. Study on the coal quality characteristics of a gas coal in Russia. Coke Chem. 68 (2), 131–135.

Isah, U.A., Rashid, M.I., Kiman, S., Idriss, I.M., Iyodo, H.M., 2025. Kinetics and heating rates effects on coal devolatilization during pyrolysis. Thermochim. Acta 748, 179999.

Jia, J., Wu, Y., Zhao, D., Wang, F., Wang, D., Yang, Q., Xing, Y., 2025. Study on combustion reaction products and free radicals of aliphatic hydrocarbon functional groups in coal based on ML potential MD. Sci. Rep. 15 (1), 10144.

Keboletse, K.P., Ntuli, F., Oladijo, O.P., 2021. Influence of coal properties on coal conversion processes-coal carbonization, carbon fiber production, gasification and liquefaction technologies: a review. Int. J.Coal Sci.Technol. 8 (5), 817–843.

Lak, S.Z., Rezaei, J., Rahimpour, M.R., 2024. Health and pollution challenges of fossil fuels utilization. Encycl. Renew. Energy Sustain. Environ 8, 155.

Li, B., Li, B., Deng, J., Gao, H., Li, Z., Xiao, Y., Shu, C.-M., 2024. Study of greenhouse gas emissions from smoldering coal fires: estimation considering the indirect greenhouse effect of precursors. J. Clean. Prod. 443, 141113.

Li, H., Hou, Y., He, Z., Wei, J., Ren, S., Wu, W., 2023. Structural evolution characteristics of lignite during pyrolysis based on alkaline-oxygen oxidation, NMR and FTIR. J. Anal. Appl. Pyrolysis 172, 105980.

Li, L., Fan, H., Hu, H., 2015. A theoretical study on bond dissociation enthalpies of coal based model compounds. Fuel 153, 70–77.

Li, S., Zeng, Y., Qu, R., Li, M., Ma, Y., Jia, X., Yu, J., Xie, Z., Tao, C., Liu, Z., 2025a. Insight into fast infrared-assisted and coal rank on pyrolysis kinetics and products distribution. J. Anal. Appl. Pyrolysis 187, 106986.

Li, Y., Yang, J., Deng, J., Zhang, Y., Yang, C., Bai, K., Pourpasha, H., Mohammadfam, Y., Heris, S.Z., Zhang, D., 2025b. Investigation of the oxidation mechanism of coal carboxyl functional groups using naphthalene acetic acid as a model compound. J. Phys. Chem. Solid., 113090

Lin, X., Wang, C., Ideta, K., Miyawaki, J., Nishiyama, Y., Wang, Y., Yoon, S., Mochida, I., 2014. Insights into the functional group transformation of a Chinese brown coal during slow pyrolysis by combining various experiments. Fuel 118, 257–264.

Ma, C., Zhao, Y., Lang, T., Zou, C., Zhao, J., Miao, Z., 2023. Pyrolysis characteristics of low-rank coal in a low-nitrogen pyrolysis atmosphere and properties of the prepared chars. Energy 277, 127524.

Mishra, S., Prasad, A.K., Shukla, A., Vinod, A., Preety, K., Varma, A.K., 2023. Estimation of carbon content in high-ash coal using mid-infrared fourier-transform infrared spectroscopy. Minerals 13 (7), 938.

Niu, Z., Liu, G., Yin, H., Wu, D., Zhou, C., 2016. Investigation of mechanism and kinetics of non-isothermal low temperature pyrolysis of perhydrous bituminous coal by in-situ FTIR. Fuel 172, 1–10.

Pan, R.-k., Li, C., Yu, M.-g., Xiao, Z.-j., Fu, D., 2020. Evolution patterns of coal micro-structure in environments with different temperatures and oxygen conditions. Fuel 261, 116425.

Pope, J., Coburn, T., Bradley, T., 2024. Committed emissions reductions available from replacement of coal-fired power plants with nuclear plants. Environ. Res.: Energy 1 (3), 035012.

Qi, X., Wang, D., Xin, H., Qi, G., 2014. An in situ testing method for analyzing the changes of active groups in coal oxidation at low temperatures. Spectrosc. Lett. 47 (7), 495–503.

Rego, F., Dias, A.P.S., Casquilho, M., Rosa, F.C., Rodrigues, A., 2020. Pyrolysis kinetics of short rotation coppice poplar biomass. Energy 207, 118191.

Ruscic, B., Wagner, A.F., Harding, L.B., Asher, R.L., Feller, D., Dixon, D.A., Peterson, K. A., Song, Y., Qian, X., Ng, C.-Y., 2002. On the enthalpy of formation of hydroxyl radical and gas-phase bond dissociation energies of water and hydroxyl. J. Phys. Chem. 106 (11), 2727–2747.

Shen, L., Fang, W.-H., 2011. The reactivity of the 1, 4-biradical formed by norrish type reactions of aqueous valerophenone: a QM/MM-based FEP study. J. Org. Chem. 76 (3), 773–779.

Shi, Q., Mi, Y., Wang, S., Cai, Y., Ji, R., Xue, W., Li, X., Han, B., 2024. Pyrolysis behavior of tar-rich coal with various coal-forming environments: a TGA and in-situ transmission FTIR study. Fuel 358, 130250.

Umar, D.F., Madiutomo, N., Monika, I., Setiawan, L., Wijaya, T., Daranin, E.A., 2024. Low-rank coal upgrading to optimize its utilization as fuel. IOP Conference Series: Earth and Environmental Science. IOP Publishing, 012031.

Vlaev, L., Markovska, I., Lyubchev, L., 2003. Non-isothermal kinetics of pyrolysis of rice husk. Thermochim. Acta 406 (1–2), 1–7.

Wang, D., 2012. The Coal Oxidation Dynamics: Theory and Application. Science Press, pp. 42–60.

Wen, L., Jin, B., Zhen-xing, G., 2011. Decomposition kinetics of hydrogen bonds in coal by a new method of in-situ diffuse reflectance FT-IR. J. Fuel Chem. Technol. 39 (5), 321–327.

Wu, M., Qin, Y., Qin, Y., Xu, N., Feng, L., 2023. The effect of temperature on molecular structure of medium-rank coal via fourier transform infrared spectroscopy. Materials 16 (20), 6746.

Xin, H., Bai, G., Wu, J., Wang, J., Yang, Y., Qi, X., Ma, L., Wang, L., Wang, D., 2024a. Stage development characteristics of oxygen-lean combustion of coal in fire zone: leap-migration mechanism, kinetic transition mechanism, and critical oxygen concentration. Fuel 377, 132799.

Xin, H., Wang, J., Tian, W., Qi, Z., Bai, G., Li, J., Yang, Y., Zhang, P., Wu, Z., Wang, D., 2024b. Exploring pyrolysis gaseous tar distribution and combustion temperature identification in coal fire. Combust. Sci. Technol. 1–21.

Xiong, G., Li, Y., Jin, L., Hu, H., 2015. In situ FT-IR spectroscopic studies on thermal decomposition of the weak covalent bonds of brown coal. J. Anal. Appl. Pyrolysis 115, 262–267.

Xu, T., Srivatsa, S.C., Bhattacharya, S., 2016. In-situ synchrotron IR study on surface functional group evolution of victorian and Thailand low-rank coals during pyrolysis. J. Anal. Appl. Pyrolysis 122, 122–130.

Xu, X., Qi, Y., Tian, L., Dou, J., Appiah, J., Wang, J., Zhu, R., Chen, X., Yu, J., 2024. Evolution of carbon structure and cross-linking structure during coking process of coking coal. J. Anal. Appl. Pyrolysis 182, 106670.

Zhang, Q.L., Li, J.Y., Wang, H.X., Liu, J.L., Zhou, J., 2024a. Kinetics of pyrolysis and computational fluid dynamics modeling of low metamorphic coal. Asia Pac. J. Chem. Eng. 19 (5), e3095.

Zhang, X., Liang, H., Lu, B., Qiao, L., Huang, G., Yu, C., Zou, J., 2024b. Stage changes in the oxidizing properties of long-term water-soaked coal and analysis of key reactive groups. Fuel 358, 130186.

Zhang, Y., Qi, X., Zhang, L., Sun, J., Bai, J., Chen, L., 2025. Generation patterns and mechanistic interpretation of PAHs during high-temperature reaction processes of coal: a case study of shuozhou long-flame coal. Fuel 387, 134426.

Zhao, J., Xiao, Y., Song, J., Lu, S., Shu, C.-M., 2023. Kinetic properties of non-caking coal spontaneous combustion by evolution of its functional groups. Fuel 354, 129428.

Zheng, Y., Li, Q., Lin, B., Zhou, Y., Liu, Q., Zhang, G., Zhao, Y., 2020. Real-time analysis of the changing trends of functional groups and corresponding gas generated law during coal spontaneous combustion. Fuel Process. Technol. 199, 106237.

Zhu, R., Shao, W., Zhang, S., Wang, Z., Lei, Z., Liu, X., Cui, P., Ling, Q., 2024. Role of calcium oxide in directional regulation microstructure of coke during high sulfur coal pyrolysis. Coke Chem. 67 (6), 359–369.